UNIVERSIDADE DO ALGARVE
UNIVERSITY OF ALGARVE

FACULDADE DE CIÊNCIAS E TECNOLOGIA
FACULTY OF SCIENCES AND TECHNOLOGY

Towards a Hydrodynamic Operational model of the Algarve Coast and St. Vincent Cape.

ERASMUS MUNDUS EUROPEAN JOINT MASTER
IN WATER AND COASTAL MANAGEMENT

MESTRADO EM GESTÃO DA ÁGUA E DA COSTA
(CURSO EUROPEU)

SURUJ RAKESH BABWAH

FARO, 2011

NOME / NAME:
SURUJ RAKESH BABWAH

DEPARTAMENTO / DEPARTMENT: –
Química, Bioquímica e Farmácia
Faculdade de Ciências e Tecnologia (FCT)
Universidade do Algarve, Portugal

ORIENTADOR / SUPERVISOR:
Flávio Martins,
AREA DEPARTAMENTAL DE ENGENHARIA MECÁNICA
UNIVERSIDADE DO ALGARVE, PORTUGAL

DATA / DATE: 22nd February 2011

TÍTULO DA TESE / TITLE OF THESIS:
Hydrodynamic Operational model of the Algarve Coast and St. Vincent Cape.

JURI:

ACKNOWLEDGEMENTS

I would like to convey my deepest and most heartfelt gratitude to the following persons for their assistance and guidance throughout my thesis and also my European experience.

To my supervisor, Dr. Flávio Martins and my unofficial co-supervisor João Janeiro, for their guidance throughout the course of this thesis. To my course coordinator Professor Alice Newton for her continued support regarding all aspects of my European experience, her continued guidance is priceless. To the European Union for sponsoring this master's study through the *Erasmus Mundus External Co-operation Window Lot 10 Scholarship Programme.* To Professor Bheshram Ramlal and Professor Micaheal Sutherland for their support in the preliminary stages after having accepted the scholarship and for guidance throughout my undergraduate studies. To the many others who have assisted me throughout the course of this body of work and those who continue to do so.

To my immediate family and friends for their continued support and assistance, who have always been there despite the thousands of miles between us, the least I can do is say thank you. And, to my friends, newly found family members who I have met on this amazing journey. With whom I have shared many wonderful and amazing experiences. Thank you (Akilah , Angelika , Baravi , Ndui, Sergei, Shine, Solomon (missing but not forgotten) , Stazi , Teferi , Tina, and Vera) all for opening your lives to me, thank you all for sharing you culture and your experiences with me.

RESUMO

Este estudo pretende implementar um modelo hidrodinâmico operacionais que podem vir a ser utilizada para projetar padrões de dispersão de vazamento de óleo e também a poluição de esgotos, e pode também ser utilizado na previsão das ondas. Um modelo de duas camadas aninhadas foi criado usando MOHID Água, que é oceano poderoso software de modelagem.

A primeira camada (pai) é usado para impor as condições de contorno para a segunda camada (filho). Isso se repetiu por dois diferentes regimes de ventos dominantes, Easterly e ventos Westerly, respectivamente.

Uma comparação qualitativa foi feita entre os dados medidos de maré e do modelo previsto dados de maré. A temperatura de superfície também foi comparada de forma qualitativa os resultados do modelo. Os resultados de ambas as simulações foram analisados e comparados com a literatura histórica. A comparação foi feita na camada superficial, profundidade de 100 metros e 800m de profundidade. Na camada superficial a primeira simulação gerado um evento de ressurgência, perto do Cabo de São Vicente e no Algarve. A segunda simulação gerado um evento não ressurgência no qual o fluxo superficial foi revertida e que a massa de água quente foi ao longo da costa algarvia e no sentido horário à noite girando em torno do Cabo de São Vicente.

Na profundidade de 100 metros para ambas as simulações, os vórtices de velocidade foram observadas perto do Cabo de São Vicente de viagem norte e sul em várias instâncias.

Em profundidade 800metre um forte fluxo oceânico foi observada em direção ao norte oeste ao longo da plataforma continental.

Keywords: modelo, previsão operacional, MOHID, aninhada, simulação

ABSTRACT

This study attempts to implement a hydrodynamic operational model which can ultimately be used for projecting oil spill dispersal patterns and also sewage, pollution and can also be used in wave forecasting. A two layer nested model was created using MOHID Water, which is powerful ocean modelling software. The first layer (father) is used to impose the boundary conditions for the second layer (son). This was repeated for two different wind dominant regimes, Easterly and Westerly winds respectively.

A qualitative comparison was done between measured tidal data and the tidal output. Sea surface temperature was also qualitatively compared with the model's results.

The results from both simulations were analysed and compared to historical literature. The comparison was done at the surface layer, 100 metre depth and at 800m depth. In the surface layer the first simulation generated an upwelling event near Cape St. Vincent and within the Algarve. The second simulation generated a non-upwelling event within which the surface was flow reversed and the warm water mass was along the Algarve coastline and evening turning clockwise around Cape St. Vincent.

At the 100 metre depth for both simulations, velocity vortexes were observed near Cape St. Vincent travelling northerly and southerly at various instances.

At 800metre depth a strong oceanic flow was observed moving north westerly along the continental shelf.

Keywords : forecasting , operational model, MOHID, nested, simulation

Contents

LIST OF FIGURES

LIST OF EQUATIONS

LIST OF TABLES

Chapter 1

1.1 Introduction

The increase of human occupation in the world coastlines makes disasters that much more devastating than in last 50 years. Many countries depend heavily upon coastal tourism, so any type of coastal disaster, natural or manmade affects the lively hood of many more people than in previous years. Also fisheries are prone to any sort of toxic spill, most notably oil spills.

Initial objectives:

To set up a pre-operational system of nested models which simulate the hydrodynamics of the Algarve Coast and St. Vincent Cape.

- Implement a set of Grids and bathymetry for the region.
- Identify operational data available and integrate it as boundary conditions for this system.
- Run model simulations for calibration purposes.
- Identify available data for model calibration.

1.2 :Project Justification

As a coastal manager it is necessary to understand the hydrodynamics that occurs within the coastal zone. Knowledge of this nature is vital in understanding pollution dispersal and the general dynamics of the location.

Hence, modelling is a vital part of this equation. Nowadays, modelling is commonly used both as a forecasting and as an investigative tool aiding the decision making process.

The modelling tool that will be developed in this thesis can also be used to implement an early warning system to predict, prevent and mitigate future problems.

1.3 :Operational Models.

1.3.1 . :State of the art

Within recent years, the importance of operational oceanography and data assimilation systems has been growing. There are many different systems and these all use varied types of data streams and have varied specific purposes. In general, they all aim to support a range of scientific and operational applications including oil spill monitoring, marine safety, and wave forecasting (Daniel P, 2005). Several European operational oceanography and data assimilation systems have been implemented in the last few years. Some examples are the POSEIDON system (Nittis *et al.* 2001) generally used for oil spills, the MOTHY model (Daniel P, 2005) created for predicting the drift of pollutants and the SHYFEM model (Bajo *et al.* 2007) utilized for storm surge prediction in Venice.

The POSEIDON system is based on OCEANOR's Sea-watch system, it was developed and operated by the Hellenic Centre for Marine Research (HCMR)(Hansen *et al.* 1997). The POSEIDON framework consists of a network comprised of 10 oceanic and 10 wave bouys deployed throughout Greece. These are all equipped with sensors necessary for monitoring the offshore environment.

Properties like wind speed and direction, air pressure and temperature, surface water temperature, sea-surface current speed and direction, wave height and direction, water temperature and salinity, dissolved oxygen, chlorophyll-a and nitrates are measured, quality controlled, stored and pre-processed in an automated way through a computing system and software present in all sensors and are near real-time remotely transmitted to

the Operational Centre of HCMR by a two-way telecommunication (http://poseidon.hcmr.gr/listview.php?id=5).

The POSEIDON system is comprised of separate but yet interrelated fractions. HCMR's Operational Centre controls and handles the surveillance of the system. The POSEIDON's forecasting ability comes from the Aegean Operational Forecasting System (AOFOS). This system is tailored to suit the Greek sea environment by means of numerical simulations and forecast models. A more detailed description is given in Nittis *et al.* (2001).The systems skeletal structure is comprised of a weather prediction model, an open sea wave forecast model, a 3D hydrodynamic model, a shallow water wave prediction model and a buoyant pollutant transport model.

The POSEIDON OSM (Oil Spill Model) can be used either in forecasting mode or hindcasting mode. The user is also allowed to input oil spill scenarios providing all the necessary parameters. The final output consists of a series of sequential graphs showing the oil spill dispersion for the requested time period (Soukissina *et al.* 2000).

1.4.1 :MOTHY MODEL

"The MOTHY model developed by Météo-France is used on an operational basis to predict the drift of pollutants on the ocean surface" (Daniel *et al.* 2005) .It is based on a hierarchy of nested limited domain ocean models coupled to a pollutant dispersion model. The model is also forced by wind and pressure fields provided atmospheric models. These atmospheric models can be the IFS model (European Centre for Medium Range Weather Forecasts) or the ARPEGE model (Courtier *et al.* 1991).

This system was specifically created to forecast drift. Currents are computed in such a way so as to represent vertical current shear. This was done by following the work of

Poon *et al.* (1991) a shallow water model coupled with a turbulent viscosity model with a bilinear eddy viscosity profile was utilized.

This approach is well suited for large areas if the major currents in the study area are considered negligible (Daniel 2005) .However if these currents have a profound impact on the dynamics of the study area, a forecaster is needed to review the forecasted data.

The oil slick itself is modelled in such a way that it considers the oil droplets to be independent and their movement is influenced by its own buoyancy and oceanic parameters such as currents and turbulence. In general 90%-95% of oil droplets remain on the surface. This is because the buoyancy is dependant upon the size and density of the oil droplets, thus larger droplets stay on the surface and the smaller ones are mixed in the upper surface layer of the water column (Comerma *et al.* 2002).The model calibration is documented in Daniel (1996). It was based upon several pollution incidents.

1.5.1 :Storm surge prediction in Venice

Although not intended for the management of the flood barriers, forecasting water levels is also important to alert businesses, warehouses and tourist-related activities of flooding events. The SHYFEM model was previously used operationally for numerically predicting storm surges in the northern Adriatic Sea.

1.5.2 :Numerical model

The Core of the forecasting system is the SHYFEM Model. It is an open source project developed at CNR-ISMAR in Venice. The code is freely downloadable from the web page: http://www.ve.ismar.cnr.it/shyfem and can be compiled under a variety of Unix and Linux like operating systems. The Shallow-water Hydrodynamic Finite Element Model (SHYFEM), developed at ISMAR-NR of Venice (Bajo *et al.* 2007) is operational at ICPSM since November 2002 (Canestrelli *et al.* 2005).

1.5.3 :Meteorological data

The European Centre for Medium-Range Weather Forecasts (ECMWF) provides the wind and atmospheric data used by the model. The Centro Nazionale di Meteorologia e Climatologia Aeronautica (CNMCA, the Aeronautic National Centre of Meteorology and Climatology of the Italian Air Force) distributes in real time the analysis and forecast fields. The centre supplies mean sea level pressure and surface wind fields over the Mediterranean area. On a daily basis a server from the CNMCA in Rome, transfers the meteorological fields to a dedicated server at the ICPSM (Bajo *et al.* 2007).

1.5.4 :The operational procedure

On a daily basis the procedure begins with a connection to a storage server of the ICPSM centre, upon which a complete data set for meteorological forcing is downloaded. Upon completion of this task, the data is then spatially interpolated to the finite element grid of the Mediterranean Sea.The forcing data is applied and simulation commences. The simulated data produces hourly forecasts with a range of up to 6 days in advance. At the end of the simulation, model results are summed to the computed astronomical tide and a prediction of the total sea level is provided (Bajo *et al.* 2007).

Chapter 2 Mohid Modelling

2.1 :Overview

This chapter describes the three-dimensional (3D) water modelling system MOHID and provides an insight on the modules used in this work. The MOHID model is being developed by a large team from the *Instituto Superior Técnico (IST),* Portugal, in close cooperation with Hidromod Lda and includes contributions from the permanent research team and from a large number of PhD students on Environmental and Mechanical Engineering from *IST* master course on Modelling of the Marine Environment. Contributions from other research groups have also been very important for the development of the model (Neves *et al.* 2003).

2.1.1 . :History

The first version of the MOHID modelling software was created in 1985. With the passing of time, the software matured with continuous updates and improvements to its use in the framework of many research and engineering projects. MOHID was initially a bi-dimensional tidal model (Neves 1985).

As part of the MOHID system other models were created, bi-dimensional euleran and lagrangian transport modules were also included with a Boussinesq model for non-hydrostatic gravity waves (Silva 1992).

Santos (1995) introduced the first three dimensional model. This model utilized a double sigma coordinate system (MOHID 3D). However, the double sigma coordinate system had many limitations. This impressed the need for a model which could use a generic vertical coordinate, allowing the user to have a choice among several coordinates, depending on the main processes in the study area (Neves 2003).

Martins (1999) answered the call for this necessity by introducing the version Mesh 3D with a generic vertical coordinate and formulated infinite volumes. In the *Mesh 3D*

model, a 3D eulerian transport model, a 3D lagrangian transport model and a zero-dimensional water quality model were included. This version of the model revealed that the use of an integrated model based on a generic vertical coordinate is a very powerful tool. However, due to the extended limitations of the FORTRAN 77 language the model was difficult to maintain. A decision was then made to reorganise the model in an object oriented architecture, using FORTRAN 95 potentialities (Neves 2003).

2.1.3 . :Mohid Program Design

Initially MOHID was a bi-dimensional tidal model developed by Neves, (1985) who applied the model in the study of estuaries and coastal areas using a classical finite-difference approach. In 1998 the whole code was submitted to a complete rearrangement with the main objective of producing a more robust and reliable model and to protect its structure against involuntary programming errors. To achieve this goal, object oriented programming using FORTRAN 95 was introduced in the MOHID model. Some of the techniques used are described in Decyk et al. (1997). The new philosophy of the model (Miranda et al. 2000) permits the use of the model in any dimension (one-dimensional, two-dimensional or three-dimensional). The whole model is programmed in ANSI FORTRAN 95, using the objected orientated philosophy.

The model was restructured and converted to ANSI FORTRAN 95, profiting from its new features such as the ability to use object oriented programming methods. Source code written according to the F95 standards assures that MOHID Framework applications can run in any operative system that supports a F95 compiler (Leitão 2003).

This migration began in 1998, implementing object oriented features as described by Decyk et al. (1997) with significant changes in code organisation (Miranda *et al.* 2000) This ultimately led to an object oriented model for surface water bodies which integrates different scales and processes The modular architecture from object-oriented model was the basis for the creation of the current which is a system of several numerical tools There are three main programs: (i) *MOHID Water,* (ii) *MOHID Land* and (iii) *MOHID Soil.*

Table 1: The three main programs n MOHID system and their generic use(Braunschweig *et al.*).

MOHID Water	It is an updated version to simulate processes in free surface water bodies .
MOHID Land	It is used to model river basins
MOHID Soil	Intended to study processes in ground water porous media(saturated and unsaturated).

Nowadays, Mohid Water Modeling System is robust and reliable system for modelling and integrated water resources management.

The FORTRAN 95 is not primarily an object-oriented language, but can be used for object-oriented programming. The modules generated in FORTRAN can be used as classes(Decyk *et al.* 1997; Akin *et al.* 2002).

The architecture of MOHID is based on different programming features. The classes that form the MOHID Framework were designed on a common basis, regarding programming rules and definition concepts in order to establish a straightforward

connection of the whole code. *"This is reflected in memory organization, public methods systematisation, possible object states, client/server relations and errors management"* (Leitão 2003).

whole model structure is divided into modules, which each respective module to feature a certain class. The table below lists and describes three such examples of different class levels.

Table 2: Different "Class" levels of MOHID (Braunschweig *et al.*).

Class name	Description	Public Information
Enter data	Reads files that have an ASCII format similar to the XML format. **Low Level Class**-used by all modules accessing the data file.	All information contained in the file
Horizontal Grid	Guards your information on a horizontal grid structure. **Intermediate level class**-used by main executable system MOHID.	Rotates the mesh area cells, details of centres of cell coordinates of the cell vertices, distance between centres,etc
Hydrodynamic	Resolve the properties non-turbulent column water bodies of water surface (eg oceans, estuaries, lagoons). High Level Class-only used in MOHID Water	Water level, field speed, and water flows between cells

The whole model is programmed in ANSI FORTRAN 95, using the objected orientated philosophy. The subdivision of the program into modules, like the information flux between these modules was object of a study by the Mohid authors.

2.2 MOHID Modules

MOHID is composed by over 40 modules which complete over 150 mil code lines. Each module is responsible to manage a certain kind of information. The main modules are the modules listed in the following table.

Table 3: List of the main modules used in MOHID. Reproduced from (Neves 2003)

Module Name	Brief Module Description
Model	Manages the information flux between the hydrodynamic module and the two transport modules and the communication between nested models.
Hydrodynamic	Full 3D baroclinic hydrodynamic free surface model. Computes the water level, velocities and water fluxes.
Water Properties (Eulerian transport)	Eulerian transport model. Manages the evolution of the water properties (temperature, salinity, oxygen, etc.) using an eulerian approach.
Lagrangian	Manages the evolution of the same properties as the water properties module using a lagrangian approach. Can also be used to simulate oil dispersion.
Water Quality	Zero-dimensional water quality model. Simulates the oxygen, nitrogen and phosphorus cycle. Used by the eulerian and the lagrangian transport modules. Based on a model initially developed by EPA (Bowie, *et. al.,* 1985) and another based on ERSEM (Baretta *et al.* 1995).
Oil Dispersion	Oil dispersion module. Simulates the oil spreading due to thickness gradients and internal oil processes like evaporation, emulsification, dispersion, dissolution and sedimentation.
Turbulence	One-dimensional turbulence model. Uses the formulation from the

	GOTM model.
Geometry	Stores and updates the information about the finite volumes.
Boundary Conditions	*Surface*-Boundary conditions at the top of the water column. *Bottom*-Boundary conditions at the bottom of the water column. *Open*-Boundary conditions at the frontier with the open sea.
Discharges	River or Anthropogenic Water Discharges

A brief description of the module utilized will be presented in the following section.

2.2.3 . Hydrodynamic Module

The hydrodynamic module solves the three-dimensional incompressible primitive equations. Hydrostatic equilibrium and Boussinesq approximation is assumed. The momentum balance equations for mean horizontal flow velocities are, in Cartesian form:

$$\partial_t u = -\partial_x(uu) - \partial_y(uv) - \partial_z(uw)$$

$$+ fv - \frac{1}{\rho_0}\partial_x p + \partial_x\left((\nu_H + \nu)\partial_x u\right) + \partial_y\left((\nu_H + \nu)\partial_y u\right) + \partial_z\left((\nu_t + \nu)\partial_z u\right)$$

Equation 1

$$\partial_t v = -\partial_x(vu) - \partial_y(vv) - \partial_z(vw)$$

$$- fu - \frac{1}{\rho_0}\partial_y p + \partial_z\left((\nu_H + \nu)\partial_x v\right) + \partial_y\left((\nu_H + \nu)\partial_y v\right) + \partial_z\left((\nu_t + \nu)\partial_z v\right)$$

Equation 2

Where u, v and w are the Reynolds averaged components of the velocity vector in the x, y and z directions respectively, f the Coriolis parameter, ν_H and ν_t the turbulent viscosities in the horizontal and vertical directions, ν is the molecular kinematic viscosity (equal to 1.3×10^{-6} m^2 s^{-1}) and p is the pressure. The temporal evolution of velocities (term on the left hand side) is the balance of advective transports (the first three terms on the right hand side), Coriolis force (forth term), pressure gradient (fifth term) and turbulent diffusion (last three terms).

The vertical velocity is calculated from the incompressible continuity equation (mass balance equation):

$$\partial_x u + \partial_y v + \partial_z w = 0$$

Equation 3

by integrating between bottom and the depth z where w is to be calculated:

$$w(z) = -\partial_x \int_{-h}^{z} u dz - \partial_y \int_{-h}^{z} v dz$$

Equation 4

The free surface equation is obtained by integrating the equation of continuity over the whole water column (between the free surface elevation η(x,y) and the bottom -h):

$$\partial_t \eta = -\partial_x \int_{-h}^{\eta} u dz - \partial_y \int_{-h}^{\eta} v dz$$

Equation 5

The hydrostatic approximation is assumed which reduces the vertical momentum equation to:

$$\partial_z p + g\rho = 0$$

Equation 6

where g is gravity and ρ is density. If the atmospheric pressure p_{atm} is subtracted from p, and density ρ is divided into a constant reference density ρ_0 and a deviation ρ' from that constant reference density, after integrating from the free surface to the depth z where pressure is calculated :

$$p(z) = p_{atm} + g\rho_0(\eta - z) + g\int_{z}^{\eta} \rho' dz$$

Equation 7

This relates pressure at any depth with the atmospheric pressure at the sea surface, the sea level and the pressure anomaly integrated between that level and the surface. By using this expression and the Boussinesq approximation, the horizontal pressure gradient in the direction x_i can be divided in three contributions:

$$\partial_{x_i} p = \partial_{x_i} p_{atm} - g\rho_0 \partial_{x_i} \eta - g\partial_{x_i} \int_z^\eta \rho' dz$$

Equation 8

The total pressure gradient is the sum of the gradients of atmospheric pressure, of sea surface elevation (barotropic pressure gradient) and of the density distribution (baroclinic pressure gradient).

2.2.4 SPATIAL DISCRETIZATION

The model uses a finite volume approach (Chippada *et al.* 1998; Martins *et al.* 2001) to discretize the equations.

In this approach, the discrete form of the governing equations is applied macroscopically to a cell control volume. A general conservation law for a scalar U, with sources Q in a control volume Ω is written as:

$$\partial_t \int_{\Omega} U d\Omega + \oint_{S} \vec{F} d\vec{S} = \int_{\Omega} Q d\Omega$$

Equation 9

Where F are the fluxes of the scalar through the surface S embedding the volume. After discretizing this expression in a cell control volume j where U is defined, we obtain:

$$\partial_t \left(U_j \Omega_j \right) + \sum_{faces} \vec{F} \cdot \vec{S} = Q_j \Omega_j$$

Equation 10

In this form, the solution for the equations is independent of cell geometry. The cell is able to take on any shape with very few constraints (Martins 1999) since only fluxes among the cell faces are required. Geometry is achieved from this because of the complete separation of the physical variables (Hirsch 1988).

The geometry is continuously updated in every time step because volumes can vary in their course of the calculus. The spatial coordinates are, independent: this means that any vertical geometry can be chosen for the mesh. Cartesian or curvilinear coordinates can be used in the horizontal and a generic vertical coordinate with different sub

domains can be used in the vertical direction (Janeiro 2006) (Figure below). This general vertical coordinate allows minimizing the errors of some of the classical vertical coordinates (Cartesian, sigma, isopycnical) as pointed in Martins et al(2001).

.

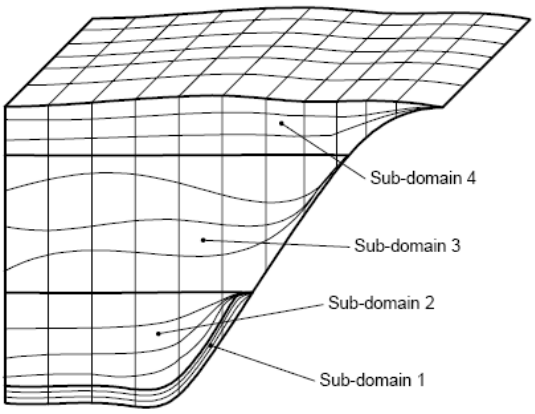

Figure 1 Illustrative grid showing the potentialities of the vertical discretization of the MOHID system adapted from Martins(1999)

Only a vertical degree of freedom is allowed, and the grid is Cartesian orthogonal in the horizontal. The grid is staggered in the horizontal in an Arakawa C manner, i.e. horizontal velocities are located in the centre of the west (u-velocity) and south (v-velocities) faces, while elevation, turbulent magnitudes and tracers are placed in the centre (Martins 1999).

Also a staggering in the vertical is used, with vertical velocity w, vertically placed in the top and bottom faces and tracers and turbulent magnitudes in the centre of the element (in vertical) (Martins 1999).

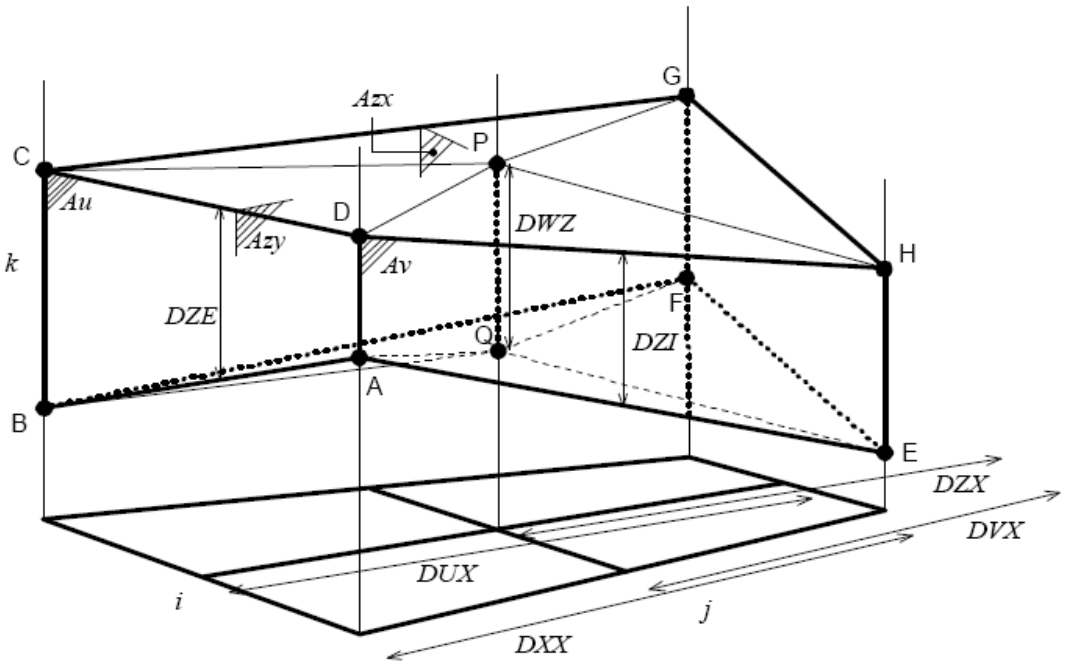

Figure 2: Volume element used in the discretization. Adapted from Martins (1999).

2.2.4.1. Temporal discretization

The temporal discretization is carried out by means of a semi implicit ADI (Alternate Direction Implicit) algorithm. This algorithm computes alternated one component of horizontal velocity implicitly while the other is calculated explicitly. The resulting equation system is a tridiagonal one, which can be solved by the Thomas algorithm in an efficient and quick way. This allows preserving the stability advantages of implicit methods without the draw-backs of computational expensiveness and associated phase errors. A longer time-step can therefore be used. A full description of the discretization may be found in Martins (1999).

2.2.5 Boundary Conditions

2.2.5.1 Free surface

All advective fluxes across the surface are assumed to be null. This condition is imposed by assuming that the vertical flux of *W* at the surface is null:

$$Wflux\Big|_{surface} = 0$$

Equation 11

Diffusive flux of momentum is imposed explicitly by means of a wind surface stress $\vec{\tau}_W$

$$\nu \frac{\partial \vec{v}_H}{\partial z}\Big|_{surface} = \vec{\tau}_W$$

Equation 12

Wind stress is calculated according to a quadratic friction law:

$$\vec{t}\omega = C_D \rho_a \vec{W}\left|\vec{W}\right|$$

Equation 13

where C_D is a drag coefficient that is function of the wind speed, ρ_a is air density and $\vec{W}$ is the wind speed at a height of 10 m over the sea surface.

Temperature and salinity advective fluxes are imposed null. Other fluxes of heat and freshwater are introduced as source/sink terms in the transport equations (described in Water Properties Module).

2.2.5.2 Bottom boundary

Also at the bottom, advective fluxes are imposed as null and diffusive flux of momentum is estimated by means of a bottom stress that is calculated by a non-slip method with a quadratic law that depends on the near-bottom velocity. So, the diffusive term at the bottom is written as:

$$\mu \frac{\partial \vec{v}_H}{\partial z}\Big]_{bottom} = C_D \vec{v}_H \left|\vec{v}_H\right|$$

Equation 14

CD is the bottom drag coefficient that is calculated with the expression:

$$C_D = \frac{k}{\log \frac{z + z_D^b}{z_D^b}}$$

Equation 15

Herein is the k the Von Karman-constant and z_D^b the bottom roughness lenth. Default values are κ = 0.4 and z_D^b = 0.0025 m. The bottom stress term is computed implicitly bin MOHID.

2.2.5.3 Lateral closed boundaries

At these boundaries, the domain is limited by land. For the spatial resolution used here this lateral boundary layer is not resolved, for that reason an impermeable, free slip condition is used:

$$\frac{\partial \vec{v}_H}{\partial n} = \mathbf{0}$$

Equation 16

$$\vec{v}.\vec{n} = \mathbf{0}$$

Equation 17

In the finite volume formalism, these conditions are implemented straightforwardly by specifying zero normal water fluxes and zero momentum diffusive fluxes at the cell faces in contact with land.

2.2.5.4 Open boundaries

Open boundaries arise from the necessity of confining the domain to the region of study. The values of the variables must be introduced there such that it is guaranteed that information about what is happening outside the domain will enter the domain in a way that the solution inside the domain is not corrupted. Several different open boundary conditions were already introduced in MOHID (Santos 1995; Martins 1999; Montero 1999).

Two methods of open boundary conditions (OBC) can be used in MOHID : radiative methods and nudging (relaxation) method).

The Dirichelet condition (clamped) can be regarded as the simplest form of active boundary condition where the field, Φ, is connected at the boundary to a reference solution, Φ_{ext},

$$\Phi = \Phi_{ext}$$

Equation 18

The concept is generalized with the linear boundary operator B, and a general class of simple active boundary condition follow the relation

$$B\Phi = B\Phi_{ext}$$

Equation 19

The particular case of the clamped condition considers B = id. When only the external water level is known, then the Blumberg method (Blumberg and Kantha, 1985), consisting of a combination between a nudging term and the Sommerfeld condition, may be used:

$$\frac{\partial \eta}{\partial t} + \vec{c} \cdot \vec{n} \Delta \eta = -\frac{\eta - \eta_{ref}}{T_{lag}}$$

Equation 20

Where T_{lag} is the relaxation decay time. For the other variables, where no accurate estimation of their celerity is available, another class of OBC method is implemented in MOHID: the relaxation method. It consists on a looser approach to the clamped (Dirichelet) conditions on the open boundary Γ of the domain Ω (Blayo *et al.* 2005)where a relaxation decay time is introduced and an additional domain is created Ωs, close to the boundary where the condition is applied. This approach is commonly regarded as a Flow Relaxation Scheme (FRS) (Martinsen *et al.* 1987). The relaxation term writes:

$$\frac{\partial \Phi}{\partial t} = -\frac{\Phi - \Phi_{ref}}{T_{lag}}$$

Equation 21

Where Φ is the relaxed variable, Φ_{ref} is the reference solution and T_{lag} is the relaxation decay time. Additionally, in order to smooth out the nudging at Ωs, a sponge layer, consisting of a high viscosity layer, can also be implemented in MOHID.

2.2.5.5 Moving boundaries

Moving boundaries are closed boundaries that change position in time. If there are intertidal zones in the domain, some points can be alternatively covered or uncovered depending on tidal elevation. A stable algorithm is required for modelling these zones and their effect on hydrodynamics of estuaries. A detailed exposition of the algorithms used in MOHID can be found in Martins(1999).

2.2.4 Water Properties Module

The water properties module computes the evolution of the water properties in the water column, using an Eularian approach. This includes the transport due to advective and diffusive fluxes, water discharges from rivers or anthropogenic sources, exchange with the bottom (sediment fluxes) and the surface (heat fluxes and oxygen fluxes), sedimentation of particulate matter and the internal sinks and sources (water quality). The model solves transport equations for salinity and temperature:

$$\partial_t S = -\partial_x(uS) - \partial_y(vS) - \partial_z(wS) + \partial_x(\nu'_H \partial_x S) + \partial_y(\nu'_H \partial_y S) - \partial_z((\nu'_t + \nu'_T)\partial_z S) + F_S$$

Equation 22

$$\partial_t T = -\partial_x(uT) - \partial_y(vT) - \partial_z(wT) + \partial_x(\nu'_H \partial_x T) + \partial_y(\nu'_H \partial_y T) + \partial_z((\nu'_t + \nu'_S)\partial_z T) - F_T$$

Equation 23

With ν'_h and ν'_t the horizontal and vertical eddy diffusivities of salt and temperature (considered to be equal), and ν'_T and ν'_s the molecular diffusivities of salt and temperature (1.1×10^{-9} and 1.4×10^{-7} $m^2 s^{-1}$). The temporal evolution of S and T is the balance of advective transport by the mean flow, turbulent mixing and the contributions of F_T and F_S, the possible sinks or sources of temperature and salinity.

The transport due advective and diffusive fluxes, of a given property *A*, is resolved by the following equation:

$$\partial_t A = -\partial_x(uA) - \partial_y(vA) - \partial_z(wA) + \partial_x(\nu'_H \partial_x A) + \partial_y(\nu'_H \partial_y A) + \partial_z((\nu'_t + \nu'_A)\partial_z A)$$

Equation 24

The density ρ is calculated as a function of temperature and salinity by a simplified equation of state (Leendertsee *et al.* 1978):

$$\rho = \frac{\left(5890 + 38T^2 + 3S\right)}{\left(1779.5 + 11.25T - 0.0745T^2\right) - \left(3.8 + 0.01T\right)S + 0.698\left(5890 + 38T - 0.375T^2 + 3S\right)}$$

Equation 25

That is an approximation for shallow water of the most widely used UNESCO equation (UNESCO 1981).

At present the MOHID model can simulate 24 different water properties: temperature, salinity, phytoplankton, zooplankton, particulate organic phosphorus, refractory dissolved organic phosphorus, non-refractory dissolved organic phosphorus, inorganic phosphorus, particulate organic nitrogen, refractory organic nitrogen, non-refractory organic nitrogen, ammonia, nitrate, nitrite, biological oxygen demand, oxygen, cohesive sediments, ciliate bacteria, particulate arsenic, dissolved arsenic, larvae and fecal coliforms. In the water quality module, the nitrogen, oxygen and phosphorus cycle can simulate the terms of sink and sources.

2.2.5 Lagrangean Module

Lagrangean transport models are very useful to simulate localized processes with sharp gradients (submarine outfalls, sediment erosion due to dredging works, hydrodynamic calibration, oil dispersion, etc.).

MOHIDS*'s* lagrangean module uses the concept of tracer, which varies according to the application of the model. For a physicist a tracer can be a water mass, for a geologist it can be a sediment particle or a group of sediment particles and for a chemist it can be a molecule or a group of molecules. A biologist can spot phytoplankton cells in a tracer (at the bottom of the food chain) as well as a shark (at the top of the food chain), which means that a model of this kind needs to simulate a wide spectrum of processes (Neves 2003).

The tracers are characterized by their spatial coordinates, volume and a list of properties (each with a given concentration). Each tracer has associated a time to perform the random movement. The tracers are "born" at origins. Tracers which belong to the same origin have the same list of properties and use the same parameters for random walk, decay, etc. Origins can differ in the way they emit tracers. There are three different ways to define origins in space:

• A "Point Origin" emits tracers at a given point;

• A "Box Origin" emits tracers over a given area;

• An "Accident Origin" emits tracers in a circular form around a point;

There are two different ways in which origins can emit tracers in time:

• A "Continuous Origin" emits tracers during a period of time;

• An "Instantaneous Origin" emits tracers at one instant;

Origins can be grouped together in Groups. Origins which belong to the same group are grouped together in the output file, so it is easier to analyze the results (Neves 2003).

The most important property of a tracer is its position (x,y,z). The major factor responsible for particle movement is generally the mean velocity. The spatial coordinates are given by the definition of velocity:

$$\frac{dx_i}{dt} = u_i(x_i, t)$$

Equation 26

where u stands for the mean velocity and x for the particle position. Velocity at any point of space is calculated using a linear interpolation between the points of the hydrodynamic model grid. The Lagrangean module permits to divide the calculation of the trajectory of the tracers into sub-steps of the hydrodynamic time step.

Turbulent transport is responsible for dispersion, the effect of eddies over particles depends on the ratio between eddies and particle size. Eddies bigger than the particles make them move at random as explained below

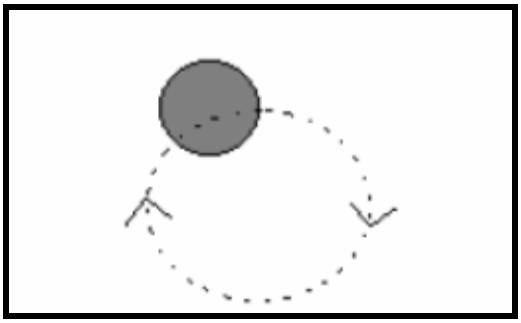

Figure 3: Random movement caused by an eddy larger than the particle

Eddies smaller than the particles cause entrainment of matter into the particle, increasing its volume and its mass according to the environment concentration, seen below.

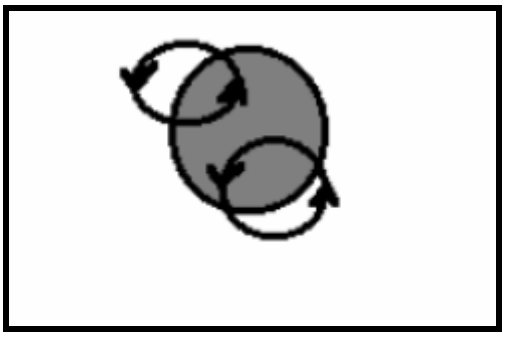

Figure 4: Random movement forced by an eddy smaller than the particle

The random movement is calculated following the procedure of Allen (1982). The random displacement is calculated using the mixing length and the standard deviation of the turbulent velocity component, as given by the turbulence closure scheme of the hydrodynamic model. Particles retain that velocity during the necessary time to perform the random movement, which is dependent on the local turbulent mixing length. The increase in volume is associated with small-scale turbulence and is reasonable to assume it as isotropic. In these conditions, small particles keep their initial shape and increase in volume as a function of its volume. To simulate oil dispersion the Lagrangean module interacts with the oil dispersion module.

2.3 Data Assimilation

"Data assimilation consists of combining the modelled fields with data observed at various points in the domain to produce the best possible estimate of the real state of the ocean over the entire model domain"(Tucker *et al.* 2004).

Numerical Weather Prediction and Ocean Prediction centres use assimilation techniques. Generally, the data prediction for the present time, is coupled with observed measurements and utilized for the next model forecast. The forecast accuracy depends upon the integrity of the present model state. This occurs because errors propagate

throughout the model. Thus, the larger the error in the earlier stages, the less accurate the forecast measurements (Kantha *et al.* 2000).

2.3.1 Continuous Assimilation

The model is kept continuously operating and data is assimilated as they become available. The fields are continuously updated to produce a nowcast. A similar model running at the same time can then produce a forecast without any data assimilation. A forecast can then be initiated at any point by a similar model running forward free without any data assimilation, but initialized from the sate of the nowcast model. Continuous assimilation has a tendency to reduce the stabilization period in the model system from the assimilation of the data. This factor makes it preferable in most cases. The principle disadvantage is the cost of running the nowcast model, in addition to the forecast model (Kantha *et al.* 2000).

2.3.2 Direct Insertion

This method is seldom used in meteorology and oceanography because the compounded errors are too great for the precise nature of metrological predictions. This method is utilized for oceanographic data because the tolerance margin for errors is greater. In this method, the model's predicted values are simply replaced by observed values at key grid points (where observation is available). The basic assumption is that the model data has too many large errors thus the observed data is accurate. A variation of this method is replacing the model generated values at grid intervals with observed data in a continuous assimilation scheme, with each input carrying its own specific weighting factor. It is expected of the model that it will be able to spread the information form observation to more nearby grid points. This method is fairly simple and thus widely utilized (Kantha *et al.* 2000).

2.3.3 Nudgeing

This method is often used in meteorology as well as oceanography. This method actually alters the governing physics and hence must be used with extreme care.

$$\frac{\partial X}{\partial t} + v \cdot \nabla X + \cdots = -\frac{(X - X_o)}{T_d}$$

Equation 27

Where the model X is nudged toward a reference value X_0 (in this case the observed value) at a timescale T_D. X_0 can itself be a function of time. The smaller the value of T_D, the more rapidly it is nudged towards the reference value, since as T_D approaches 0 , X approaches X_0 .

2.3.4 Kalman filter

The Kalman filter is very powerful in several aspects. It is a set of mathematical equations used to compute the errors inherent in a system. This filter supports estimations of past, present and future states. The Kalman filter estimates a process by using a form of feedback control: the filter estimates the process state at some time and then obtains feedback in the form of (noisy) measurements. This filter computes the process state at a specific time period and then obtains measurements in the form of feedback (noisy measurements). Because of this, the equations for the Kalman filter fall into two specific categories: time update equations and measurement update equations(Welch *et al.* 2006).

The time update equations are responsible for present case scenarios and forecasting. It is also responsible for the error covariance estimates used to obtain the a priori estimates for the next time step(Welch *et al.* 2006).

"*The measurement update equations are responsible for the feedback*"(Welch *et al.* 2006). This basically means that these equations are responsible for making the necessary corrections to the data. A more detailed explaination of the Kalman filter and the associated formulae can be found in Welch *et al.* (2006).

2.4 Applications

The MOHID model has been applied to several coastal and estuarine areas and it has showed its ability to simulate complex features of the flows. Several different coastal areas have been modelled with MOHID in the framework of research and consulting projects. Along the Portuguese coast, different environments have been studied, including the main estuaries (Minho, Lima, Douro, Mondego, Tejo, Sado, Mira, Arade and Guadiana) and coastal lagoons (Ria de Aveiro and Ria Formosa), (Martins *et al.* 2001).

The model has been also implemented in most Galician Rías: Ría de Vigo by Taboada *et al*. (1998), Montero, (1999) and Montero *et al*. (1999), Ría de Pontevedra by Taboada *et al.* (2000) and Villarreal *et al.* (2000) and in other Rías by Pérez Villar *et al* (1999).

Besidesthe Iberian Atlantic coast, some European estuaries have been modelled: the Western Scheldt in the Netherlands, Gironde in France by Cancino and Neves, (1999) and Carlingford, Ireland, by Leitão, (1997) - as well as some estuaries in Brasil (Santos SP , Fortaleza and Lagoa dos Patos). Regarding to open sea, MOHID has been applied to the North-East Atlantic region where some processes including the Portuguese coastal current, Coelho *et al.* (1994), the slope current along the European Atlantic shelf break, Neves *et al*. (1998) and the generation of internal tides, Neves *et al*. (1998) have been studied and also to the Mediterranean Sea to simulate the seasonal cycle, Taboada, (1999) or the circulation in the Alboran Sea, Santos, (1995). More recently MOHID has been applied to the several Portuguese fresh water reservoirs Monte Novo, Roxo and

Alqueva, (Braunschweig, 2001), in order to study the flow and water quality (Neves 2003).

CHAPTER 3 : SITE DESCRIPTION

3.1 Iberia

The Iberian peninsulas are characterized by their offshore activity. There is a slow broad equatorward gyre wind direction during a substantial part of the year (in some places permanently).The direction of these winds force an offshore Ekman transport in the upper layer and thus a consequent decline of the sea level towards the coast. These factors create a jet stream of water transporting cold and nutrient rich upwelled water in the direction of the equator (Relvas *et al.* 2007).

In the case of the North Eastern Atlantic system (Fig. below), the Canary and Iberian regions form two distinct subsystems (Barton 1998). The separation extends beyond geographical characteristics .It is a consequence of the distinctive characteristics of this Northeastern Atlantic region, the discontinuity is imposed by the entrance to the Mediterranean Sea (Relvas *et al.* 2007).

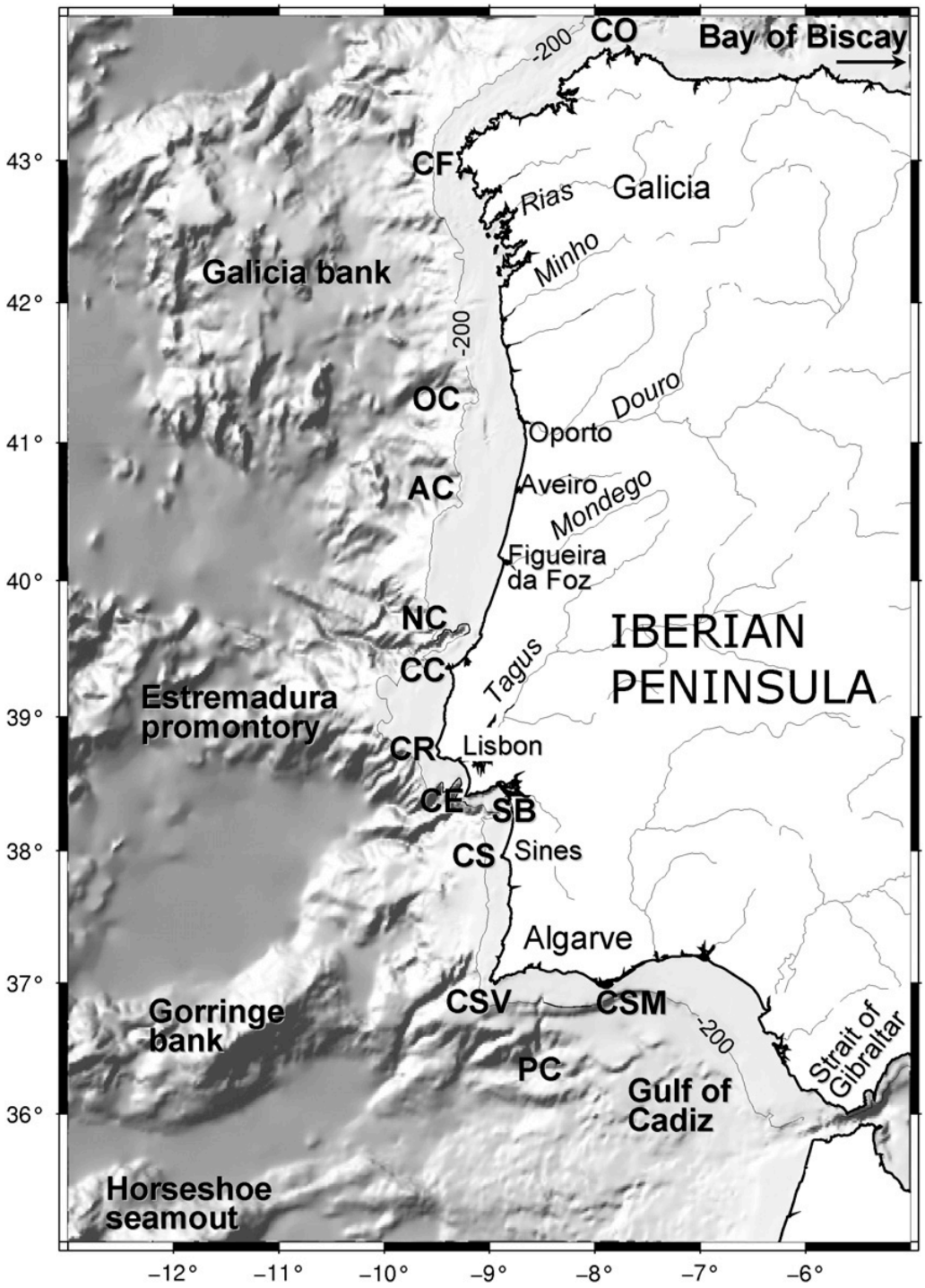

Figure 5: Geography of the Western Iberian system, showing the main features referred to in the text. The 200 m bathymetric contour, that roughly delimits the continental shelf, is represented. From north to south: CO, Cape Ortegal; CF, Cape Finisterre; OC, Oporto Canyon; AC, Aveiro Canyon; NC, Nazare´ Canyon; CC, Cape Carvoeiro; CR, Cape Roca; CE, Cape Espichel; SB, Setu´bal Bay; CS, Cape Sines; CSV, Cape Sa˜o Vicente; PC, Portima˜o Canyon; CSM, Cape Santa Maria.(Relvas *et al.* 2007)

The Azores Current extends eastward separating the oceanic gyre circulation regime into the north (Portugal Current) and the South (Canary Current) (Pollard *et al.* 1985).It is theorized that the Mediterranean outflow has a dynamic impact in the upper layer of the ocean and may constitute a complimentary mechanism for the formation of the Azores current (Jia 2000).

"The seasonal interplay of the large scale climatology between the Azores high pressure cell, strengthened and displaced northward during the summer, and the Iceland low, weakened at that time, governs the set up of upwelling favourable winds (northerlies) off western Iberia between April and October" (Wooster *et al.* 1976). There is an association between the separation of the subsystems and the sharp seasonality of the western Iberia system. The author goes on to say that this is also mainly due to the annual cycle of the atmospheric systems.

In the summer months, there is a thermal low over central Iberia, this in turn strengthens the upwelling winds. During the winter periods, the direction of the dominant wind changes and thus poleward flow becomes an outstanding feature at all levels between the surface and the Mediterranean water at approximately 1500 m, along the Iberian shelf edge and slope (Relvas *et al.* 2007).

The water transported in the surface, poleward flow is relatively warm and saline. This is identifiable in sea surface temperature satellite imagery (Haynes *et al.* 1990; Peliz *et al.* 2005)this extends as far north as the Cantabian coast and the Goban Spur (Pingree 1993.).

The wind regime for this period is reversed, so now it has a southerly component (Frouin *et al.* 1990),coupled with the meridional density gradient and the continental slope and shelf are attributed to this poleward flow (Peliz *et al.* 2003).

It is uncertain whether the surface signal of the poleward flow is maintained during the summertime simultaneous with the coastal upwelling jet (Peliz *et al.* 2005). *"The poleward flow shows a turbulent character, with eddies and smaller scale instabilities typically being generated in the shear regions"* (Peliz *et al.* 2003).

The continental shelf is approximately 610 km wide south of Lisbon, 30–40 km wide off central Portugal and somewhat narrower again off northern Portugal and Galicia (Relvas *et al.* 2005).According to Relvas *et al.* (2005) the region is filled with topographic structures such as capes, promontories and submarine canyons with spatial scales from tens to hundreds of kilometres.

The oceanography of this region is largly dominated by medium size structures that represent the "weather" variability of the ocean. The variability of the alongshore windstress is also a major governing factor or coastal circulation (A lvarez-Salgado *et al.* 2003) . The oceanographic patterns in the Iberian system reveal a multitude of structures such as jets, meanders, ubiquitous eddies, upwelling filaments and countercurrents superimposed on the more stable variations at seasonal timescales (Relvas *et al.* 2005).

3.2 Algarve

The Algarve is the south-western corner of the Iberian Peninsula. The Algarve Margin is located between 36°–37°N and 7°50–9°25 W. The Algarve coast line stretches about 160 kilometers from the western-most tip to the Spanish border. It is characterized by a rough morphology underlined by the presence of canyons, channels and contourite drifts (Salles *et al.* 2007).

Figure 6: Showing the study area. (source: Google Earth 2010)

Circulation along the Algarve coast has been the primary subject of several scientific publications. In the last decade these studies have been mainly focuses on surface variability associated with upwelling events (Relvas *et al.* 2002) also including the Mediterranean Water (MW) Undercurrent(Serra *et al.* 2005). So far, the actual physical force that generates this counter current has not been identified.

Along the Algarve coast, a coastal counter flow is frequently observed. This is frequently observed in periods of upwelling relaxation, trapped between the coast and a well established upwelling jet (Relvas *et al.* 2005).The actual physical forcing behind the generation of the counter current is not yet clear. This current is similar to others observed on the California coast and the forcing mechanism may be the spatial

variability of upwelling intensity (Harms *et al.* 1998), wind curl near the coast or a pressure gradient (Ramp *et al.* 1998) along the coast.

The Portugal Current itself (Martins, 2002; Pérez, 2001) is poorly defined spatially because of the intricate interactions between coastal and offshore currents, bottom topography, and water masses. The system is comprised of the following main currents:
The Portugal Current, which is a broad, slow, generally southward-flowing current that extends from about 10°W to about 24°W longitude;
The Portugal Coastal Counter current (PCCC), a southward flowing surface current along the coast during down welling season, mainly over the narrow continental shelf to about 10-11°W longitude and flow from about 41-44°N;
The Portugal Coastal Current (PCC), a generally poleward current that dominates over the PCCC during times of upwelling and like the PCCC, extends to about 10-11°W from shore, also present mainly from 41-44°N, where flow is 13.5 ± 5.7 cm s-1 (Pérez *et al.* 2001; Martins *et al.* 2002). The Portugal current as represented by the Mariano Global Surface Velocity Analysis (MGSVA). The average flow is towards the south and feeds the Canary Current.

Figure 7 below shows the average velocity field in the northeast Atlantic as derived from near-surface drifters. The arrow's origin is located at the average drifter positions in each box, and its length is directly proportional to the velocity magnitude. The ellipses indicate the principal directions of variance, and the correspondent axes indicate the errors. The arrow corresponding to a 10 cm s_1 mean velocity and a linear segment of 10 cm s_1 for the error are indicated on top of the figure. The number of drifter days

used in the averages is indicated on the upper left corner of each box whose geometry is variable in order to improve statistical reliability(Martins *et al.* 2002).

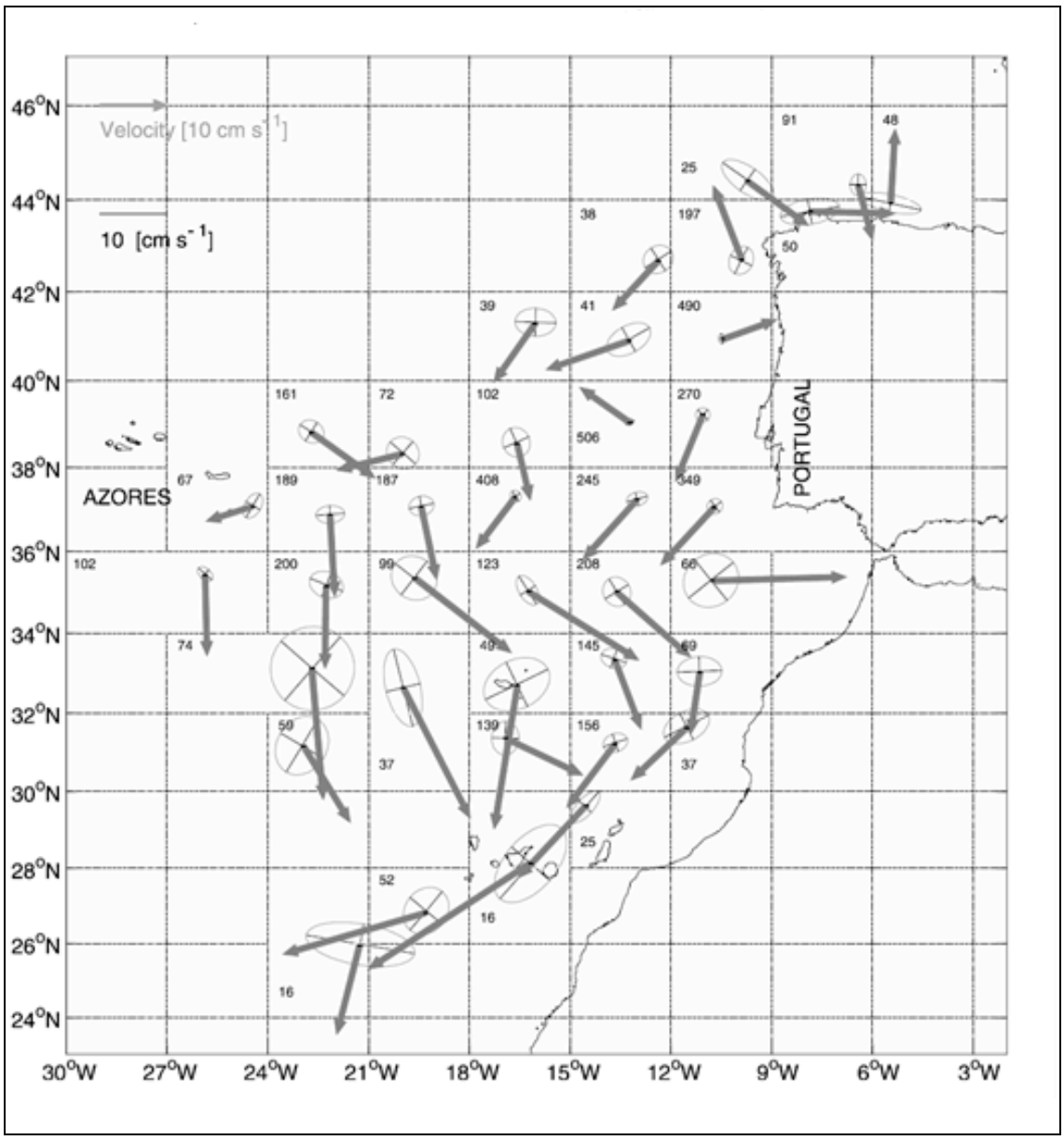

Figure 7 Surface Circulation on The Eastern North Atlantic (Martins *et al.* 2002)

The Portugal currents, has the mean pattern as well as seasonal variation and are well established despite relatively few systematic observations. The Portugal and Canary

Generally, the mean flow on the surface is southward, however seasonal winds in the region can result in both northward and southward flows, which were observed with drifters equipped with holey sock drogues centred at about 15 m over a period of 14.4 years (Martins *et al.* 2002)

3.2.3 Tidal Regime

The tidal regime is semidiurnal and mesotidal with tides ranging from 2.70 to 1.36 m during neap tides and from 3.82 to 0.64 m during spring tides (Vilamoura tide gauge). The mean rate of relative sea-level rise has been estimated as 1.5 ± 0.2 mm/yr according to data from the Lagos tide gauge's series registered between 1908 and 1987 (Dias *et al.* 1992 ; Moura *et al.* 2006).

3.2.4 Upwelling

Predominant trade winds from the north, cause wind driven upwelling along the coast of the Iberian Peninsula during the summer months. Cooler water from depths of 100-300 m is upwelled (Smyth *et al.* 2001; Bischof *et al.* 2003).These events usually begin around and are particularly intense off of Cape Finisterre and Cabo da Roca, often forming filaments that can reach as far as 100 km westward (Cuehlho *et al.* 2002; Huthnance *et al.* 2002; Bischof *et al.* 2003)and their velocities, tracked by thermal features in satellite images, can reach up to 0.28 m s^{-1} (Smyth *et al.* 2001) .

Studies of Upwelling in the Portuguese coastline have been done and papers have been published on the same topic by authors such as (Relvas *et al.* 2002; Sofia *et al.* 2005; Santos *et al.* 2001). Upwelling responds quickly to northerly winds, particularly south of capes, appearing first along the coastline and then spreading offshore as the event progresses (Fiúza 1983).

The Portugal Coastal Countercurrent (PCCC) during times of upwelling and like the PCCC, extends to about 10-11°W from shore, also present mainly from 41-44°N, where flow is 13.5 ± 6 5.7 cm s-1 (Pérez *et al.* 2001; Solignac *et al.* 2008) . The Portugal Current system is supplied mainly by the intergyre zone in the Atlantic, a region of weak circulation bounded to the north by the North Atlantic Current and to the south by the Azores Current (Pérez *et al.* 2001). For some part of the year the north-east Trade Winds blow along every part of the subtropical Eastern boundary with a strong alongshore component that produces offshore Ekman transport in the surface layers and therefore upwelling at the coast (Barton 2001).

The strength of upwelling is conventionally expressed in terms of the upwelling (or Bakun) index, which is simply the Ekman transport

Equation 28

$$TE = (q/o f)$$

where **q** is the component of wind stress parallel to shore, **o** is the density of sea water, ***f*** is the Coriolis parameter (Barton 2001) refer to figure below.

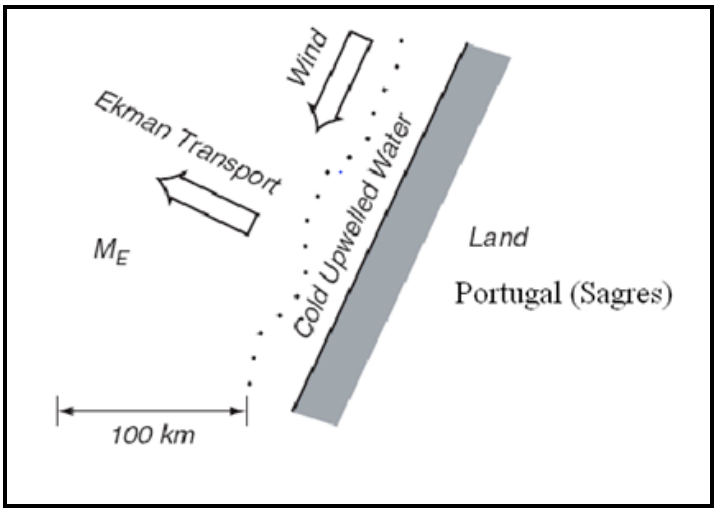

Figure 8 : Showing coastal upwelling along the Sagres coastline SW-Portugal (Source Microbiology procedure (http://www.microbiologyprocedure.com/microbial-ecology-of-differentecosystems/marine-ecosystem-upwelling.html) accessed07/05/2010

Oceanographers have long sought to verify the theoretical Ekman transport relation, which predicts that a steady wind stress acting together with the Coriolis force will produce a transport of water to the right of the wind (Price *et al.* 1987).

Off the coast of Portugal, upwelling can be found south of 40º N during summer and autumn; between 40ºN and 43ºN the upwelling period decreases with increasing latitude. The yearly amplitude of differences of sea level pressure normal to the coast which represents the synoptic scale coast parallel wind component and offshore surface temperatures is largest in 38ºN, decreasing to the north. From empirical orthogonal functions it is suggested that off Portugal local winds induce a more intense upwelling than the winds off Northwest Africa (Detlefsen *et al.* 1980) Local winds, the continental-shelf/upper-slope bathymetry and the coastal morphology largely determines the upwelling patterns off Portugal (Fiúza 1983).

Sousa *et al* (1992) concluded that upwelling took place seasonally along the west coast of Portugal. Upwelling would reach its maximum in July, August and September. This

usually occurs under fairly steady northly winds ands that its intensity presented a strong correlation with the north-south wind stress.

3.3 Cape St. Vincent

The western Iberian Peninsula (IP) is located in the northern limit of the Eastern North Atlantic Upwelling Region. Geographically, the zone is characterized by the presence of Cape St. Vincent, where the western and southern coasts intersect at an almost right angle. This cape is the most south-western point in Portugal .The 25 km wide southern shelf slopes gently down to a sharp edge at 100–130 meters depth, defined by a sudden step down to the 700 m contour. This pronounced feature extends around the southwest tip of Portugal, reaching about 10 km north of Cape St. Vincent. The shelf off the west coast of Algarve is steep and only 10 km wide (Leal 2005).

The oceanographic system off of the south-western Iberian Peninsula is still not very detailed. This system forms part of the northern tip of the Eastern Boundary Current System (EBCS) of West Europe and Northern Africa. The abrupt coastline changes at Cape Finisterre and Cape St. Vincent introduce a source for sharp geographical shifts that have an influence on the oceanographic setting.

At these sites the west coast interacts almost at right angles with the North and South Iberian coasts respectively, which confers a particular meridional symmetry in this region. This meridional symmetry is also observed with the existence of two large bights where vivid recirculation's occur, namely the Gulf of Cadiz at the south (Sanchez *et al.* 2003) and the Bay of Biscay at the north (Pingree *et al.* 1990; Leal 2005).

Sanchez and Relvas (2003) presented a comprehensive review about the average summer circulation. They noted that during the summer season there is an upwelling of colder subsurface eastern North Atlantic Central Water over the shelf and slope. Their

transport analyses observe that at times, the equatorward upwelling jet sometimes had a vigorous interaction with the offshore circulation.

Leal (2005) inferred that there were two man mechanisms: one associated with recirculation of 0.6 Sv (1 Sv=106 m^3s^{-1}) with a northern branch of the Azores Current in the vicinity of Cape St. Vincent; the other consists of cross-shelf exchanges effected by persistent upwelling filaments.

Work based on scatterometer winds have evidenced strong similarity of the winds that fall within the vicinity of the most prominent capes along the Iberian Peninsula, Cape Finisterre (Torres *et al.* 2003) and Cape St. Vincent.

The seasonal alteration of wind driven flows in the upper surface (400m), is a characteristic of the ocean. Sanchez *et al*(2003) showed proof of the mesoscale nature of flows in the western Iberian Peninsula, in summertime and in winter (Peliz *et al.* 2005).

The classical view of upwelling circulation is also featured in the climatological features (Sanchez *et al.* 2003).A cold upwelling jet extending over the upper 100 meter or more of the water column advects 1 Sv of low-salinity water equatorward.

This climatological circulation also revealed interplay between the offshore field and the pure upwelling circulation. The recurrent activity of upwelling filaments are one of the most active mechanisms in the system. Upwelling filaments are cold-water tongues, with source in the upwelling zone. They may reach some 50 km of width and several hundreds of km of length (Leal 2005).

They have been extensively studied in the west US coast, where a number of intensive observational programs have developed since the early 80's (Leal 2005). The theories for their formation in the west US coast were reviewed by (Strub *et al.* 1991).

Cold filaments are part of a continuous, meandering, southward jet with core speeds in excess of 0.5 $m \cdot s^{-1}$ over a surface layer of 100 m. As the jet meanders onshore it has cold upwelled water which is carried with the jet as it then meanders offshore (Leal 2005).

Upwelling and the associated filaments over the Iberian coastal transition zone were statistically studied by Haynes et al.(1993).This study was then extended to encompass Cape St. Vincent by Relvas (1999). It was indicated by these authors that typically the upwelling season starts in May-June, when a cold band, which is frequently populated with narrow fingers develops along the coast of the Iberian Peninsula. The filaments become common around the start of July, when they have a mean (maximum) length of 80 (120) km (minus the 50 km width of the coastal upwelling band)(Leal 2005).

Filament growth is not always continuous, and instead consists of periods of active growth interrupted by episodes when upwelling ceases. Controversy exists on which are the processes (Leal 2005) that module the formation, maturation and decay of upwelling filaments in the Iberian Coastal Transition zone.

CHAPTER 4: Simulation Implementation

The MOHID – model will have to be forced with external data in order to deliver accurate results for the hydrodynamics in the study region. The figure below gives a schematic overview of the different data forcing the model, where in the model they will be applied and the type of results delivered by the model.

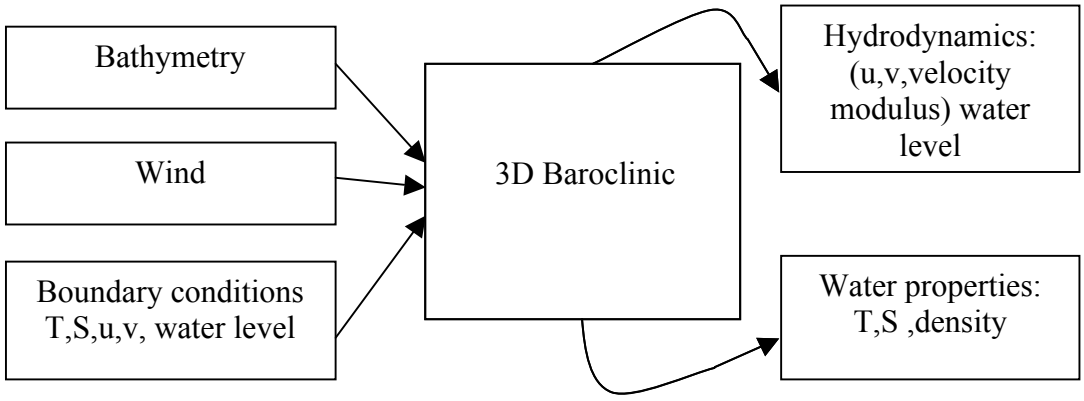

Figure 8: Schematic overview of the input data, the MOHID - model and the model's output

The data input into the model are briefly described below

4.1 . Data Description

4.1 .1Bathymetry

The General Bathymetric Chart of the Oceans (GEBCO) consists of an international group of experts who work on the development of a range of bathymetric data sets and data products, including gridded bathymetric data sets, the GEBCO Digital Atlas, the GEBCO world map and the GEBCO Gazetteer of Undersea Feature Names. The grid resolution used for the son model was 1km. (http://www.gebco.net/data_and_products/)

4.1.0 .2. Boundary Conditions.

The PCOMS model consists of a downscaling of the Mercator-Ocean PSY2V3 North Atlantic solution for the Portuguese coast, where the FES2004 tide solution is added, and the surface forcing is performed using the atmospheric forecasts from the 9 km resolution MM5 model run at IST (http://meteo.ist.utl.pt). The model was run in full baroclinic mode with a horizontal resolution of 6 km and with 50 vertical levels with a resolution of down to 1 m near the surface.

4.1.0.3. Wind

The PSU/NCAR mesoscale model (known as MM5) is a limited-area, nonhydrostatic, terrain-following sigma-coordinate model designed to simulate or predict mesoscale atmospheric circulation. MM5 meteorological surface forecasts are automatically being delivered to MARETEC (Marine Environment and Technology Center) in MOHID-HDF5 format.

4.2 . Method (Structure of the model and boundary conditions)

MOHID allows the user to construct a tree of one-way nested models with no limitations on the number of nesting levels from the software point of view.

The modelling experiments carried out in this work consisted in the use of two models: one for the entire system (father model), and a submodel of the study area (son model) with a more refined grid.

The connection between the two models was made using a one-way downscaling scheme (nested models).

The father model, which utilized a less refined grid, was used as the base for the hydrodynamic and water properties. Thus, supplying the boundary conditions needed for the son model.

The communication between the father and son models was made with the relaxation of the solutions in a band of cells of the father model, which were assimilated by the son model. The information exchange was only in one direction, from the father to the son model.

Thus, the model was forced using the boundary conditions obtained from the father model. Commands were entered into MOHID by means of the various modules utilized by the software. The Turbulence module was set to utilize GOTM for its calculations and the Geometry to be comprised of a total of 46 layers.

Geometry

The MOHID system employs a finite-volume approach for spatial discretization. In this way, it is possible to explicitly impose any kind of vertical discretization. A z-level vertical discretization was adopted with 46 layers (39 cartesian and 7 sigma) for this model. The layer thickness increases from the surface to the bottom (Leitão *et al.* 2005).

Turbulence model

GOTM is the abbreviation for General Ocean Turbulence Model .The turbulent transport of momentum, mass and heat in Mohid can be calculated in a simplified way using constant diffusion coefficients. It is a one- dimensional water column model for the most important hydrodynamic and thermodynamic processes related to vertical mixing in natural waters. In addition, it has been designed such that it can easily be coupled to 3-D circulation models, and used as a module for the computation of vertical turbulent mixing. The core of the model computes solutions for the one-dimensional versions of the transport equations of momentum, salt and heat. The key component in solving these equations is the model for the turbulent fluxes of these quantities (Burchard *et al.* 2007).

The first run of each new simulation was done with a cold start, and imposing the wind data over a period of time rather than instantly for stability purposes. The cold start implies that the model starts without any previous results as its starting point. The second run is then done as a continuation of the first, thus making it a hot start. This run continues its computation using the data from the cold start as a starting point.

This method was repeated using two separate sets of forcing data.The first simulation was done from the 8^{th}-17^{th} June 2010.The second simulation was done using data from the 3^{rd}-12^{th} July 2010.

CHAPTER 5 : RESULTS

In this section the results obtained for the hydrodynamics and water properties of the Algarve are presented. The simulations were carried done with two different wind conditions. The simulation with westerly wind was June and easterly wind was July

5.1 . JUNE

5.1.2 . Tide:

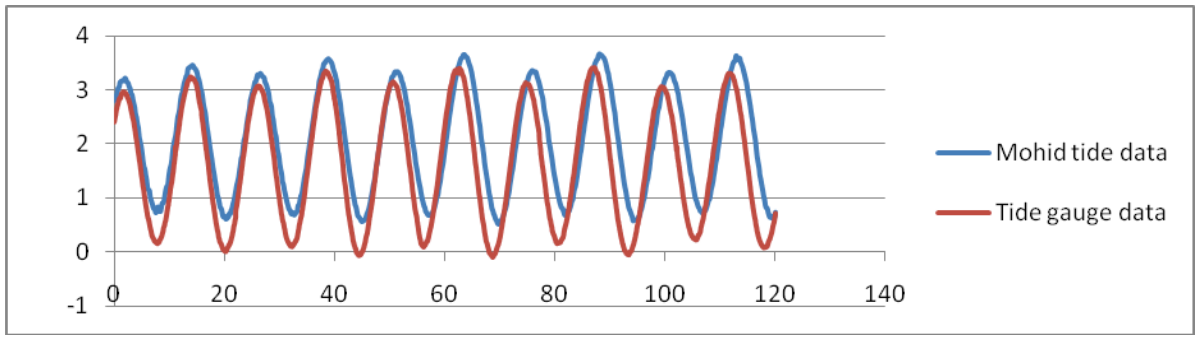

Figure 9: Graph Comparing Predicted tidal data against Measured tidal data from Lagos station.

The figure above shows tidal data from the 12th-17th of June. No tidal data was available for the simulation period beginning before this date. There are differences as large as.5m at points along the graph. The tidal data was obtained from IOC Sea Level Data Facility. They provide real time data for various tidal gauges throughout Europe.

5.1.2 Surface Layer

Upwelling

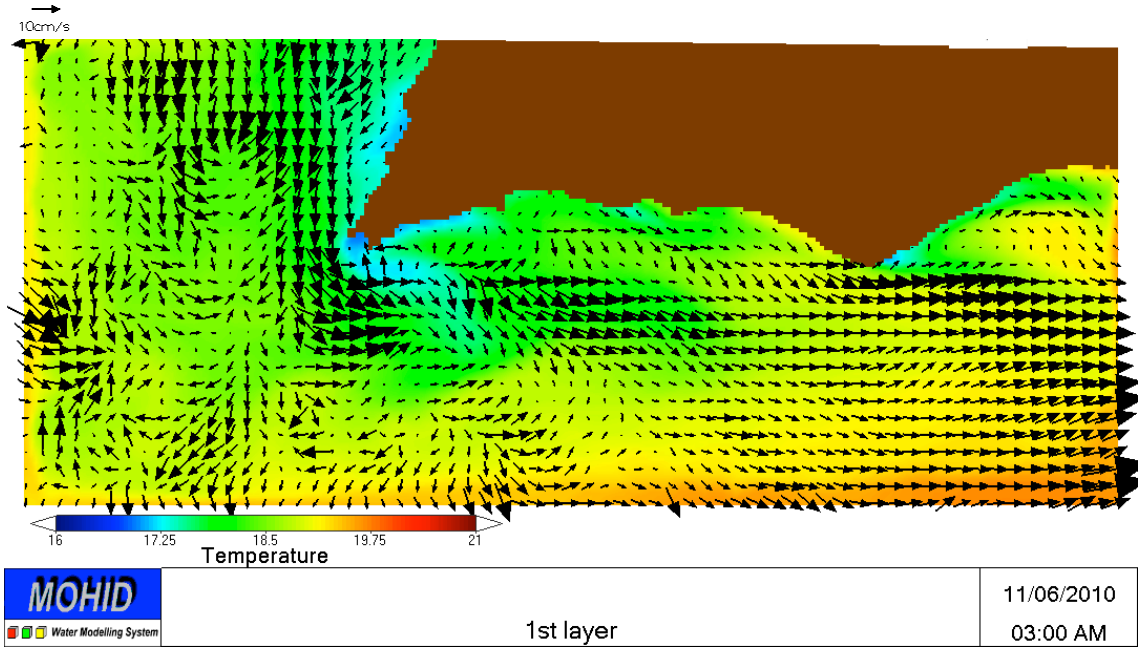

Figure 10 : Hydrodynamics of the Algarve plotted upon the water temperature.

Figure 10 shows the result after 4 days of easterly wind. At this instant, it was the strongest point during the upwelling period. It can be seen that by Cape St. Vincent and in Algarve there seems to be a concentration of colder water moving in an easterly direction. The upwelling progression can be seen in Appendix 1

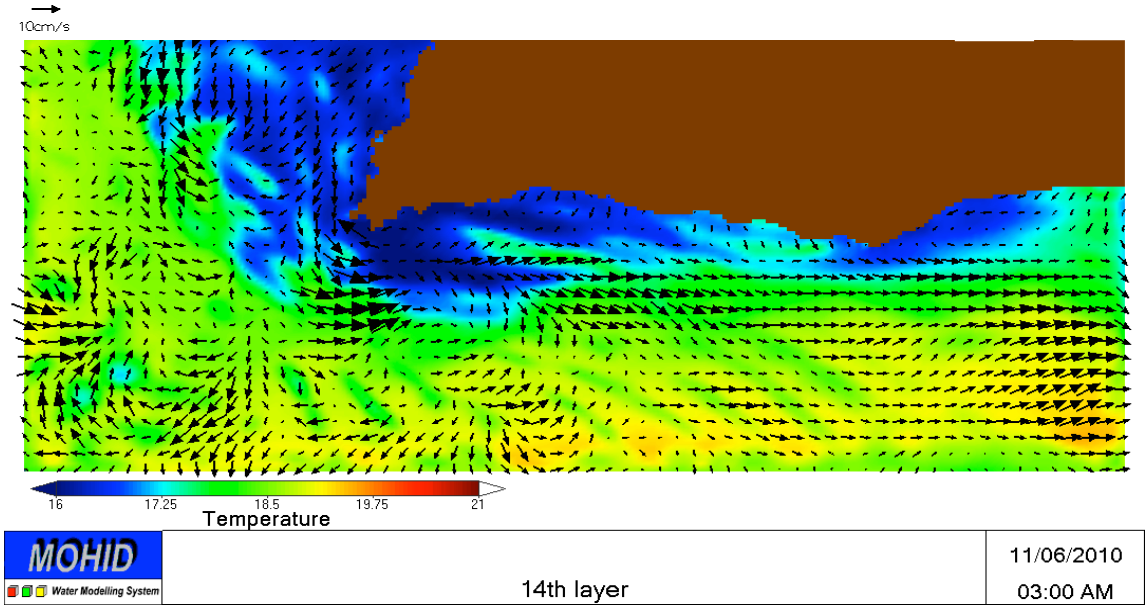

Figure 11: Depth of appromiately 25m

Figure 11 gives a better physical view of the regions of colder water masses. The velocity fields nearer to the coastline all seem to show a general movement of the water mass towards the east.

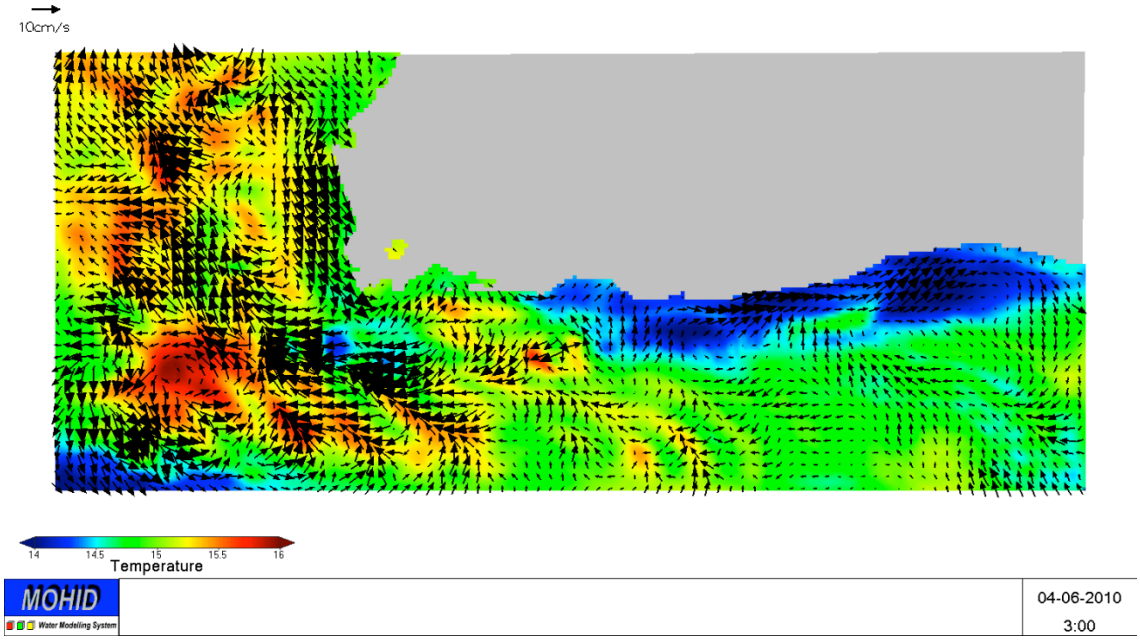

Figure 12: approximately 100m depth

This time instant was taken from the earlier stages of the simulation. Just near the coast of Cape St. Vincent there seems to be two bodies of water travelling in opposite directions. The region closer to the coastline moves south along the coastline and around cape St. Vincent and close to this region the other water mass seems to turn from a general westerly direction to more north-west. This was also observed at other instances throughout the simulation period.

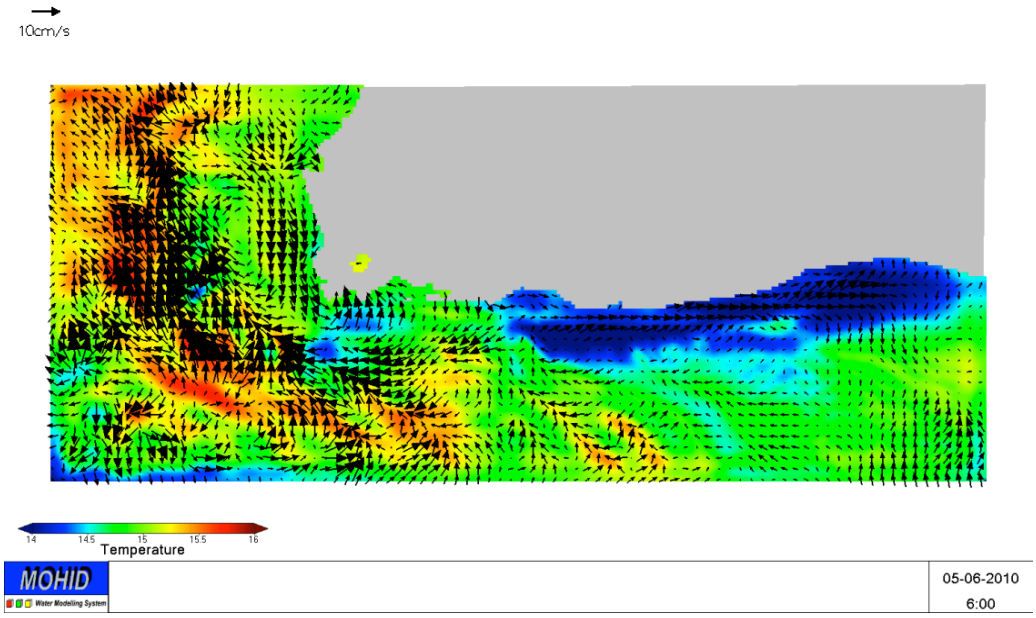

Figure 13: approximately 100m depth

Figure 13, which was also generated at a depth of 100m, shows a velocity vortex close to Cape St. Vincent. This velocity vortex was generally seen developing after situations of opposing currents occurred as shown in Figure 12. This velocity vortex was seen moving northerly and other times southerly before dissipating. The spatial progression of this velocity vortex can be seen in Appendix 2.

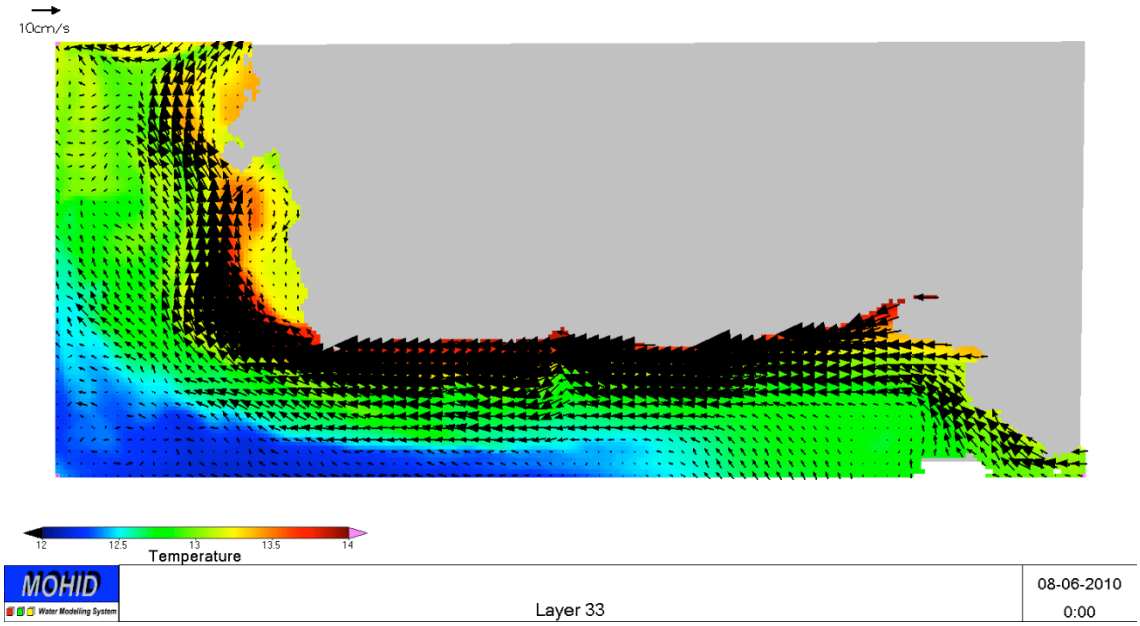

Figure 14 :800 m

Figure 14 which shows the hydrodynamics at a depth of approximately 800m was a typical representation of the model results for the entire simulation. There was always a strong velocity trend noted closer to the coastal boundary moving from the south east corner of the study to the north west. At the south east corner of the image what appears to be weak a weak velocity vortex was observed. This vortex was observed on several occasions throughout the simulation period but never lasting more than 9 hours.

JULY

Tide data

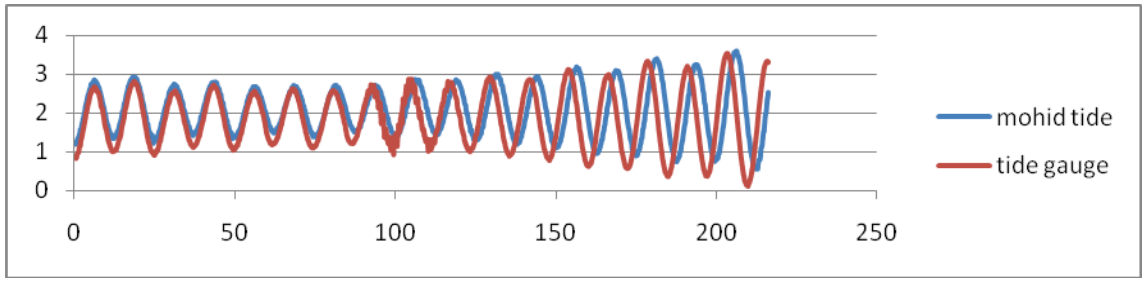

Figure 15: Tidal data comparison between mohid predicted tide and tide gauge data from Lagos.

The graph shows the beginning of the simulation from July 3rd-12th 2010. Y-axis is in meters and x-axis is in hours.The maximum difference between these two graphs were approximately .4m .

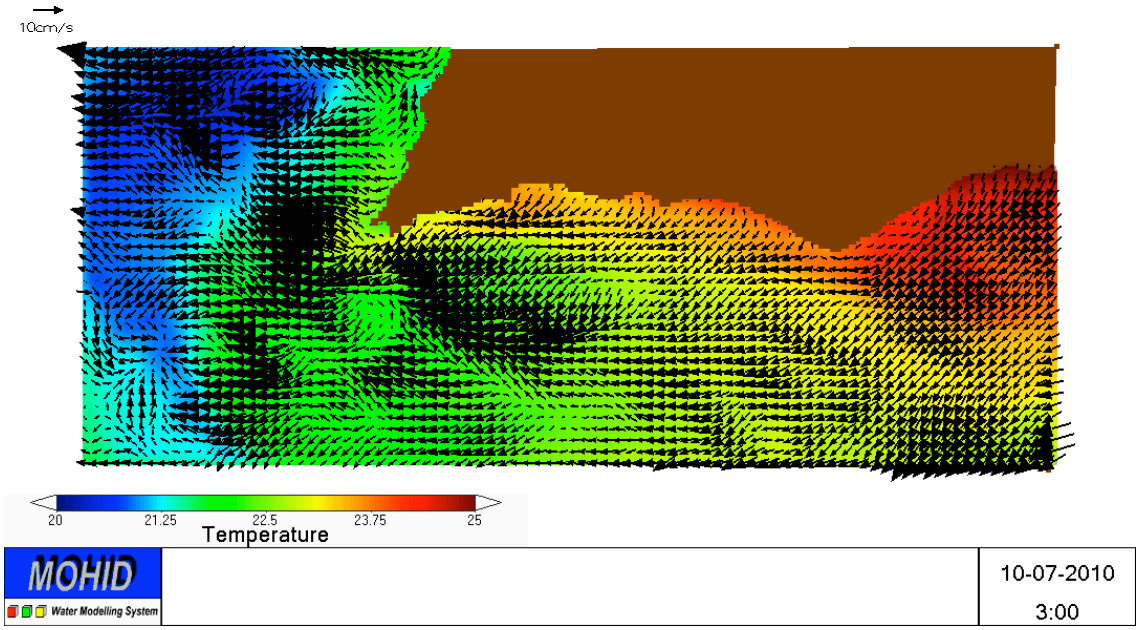

Figure 16 top layer

Figure 16 shows the result after 3 days of easterly and north easterly dominant winds. The hydrodynamics show a general westerly movement of the surface water.The image also shows warmer water originating from outside of the study area coming into the system and moving along the coast line and around the St. Vincent Cape.

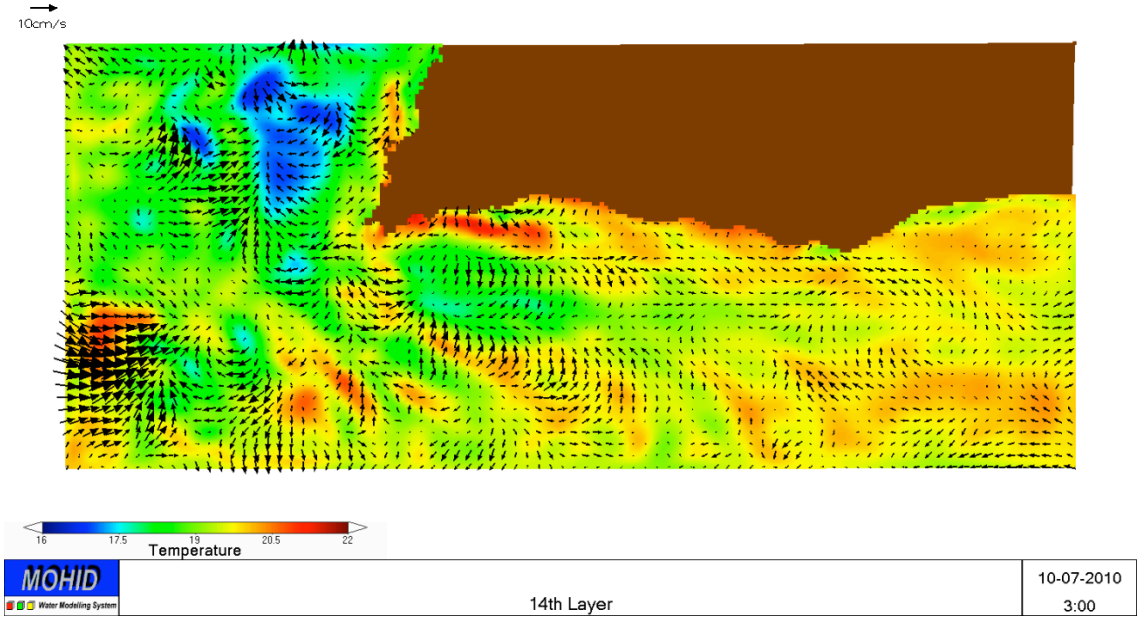

Figure 17: 25m depth

At this depth it is observed that warmer water is being pushed along the coastline but the hydrodynamics of the region are not nearly as uniform as seen in the previous figure. Warmer water is still present along the coastline and is seen curling around Cape St. Vincent.

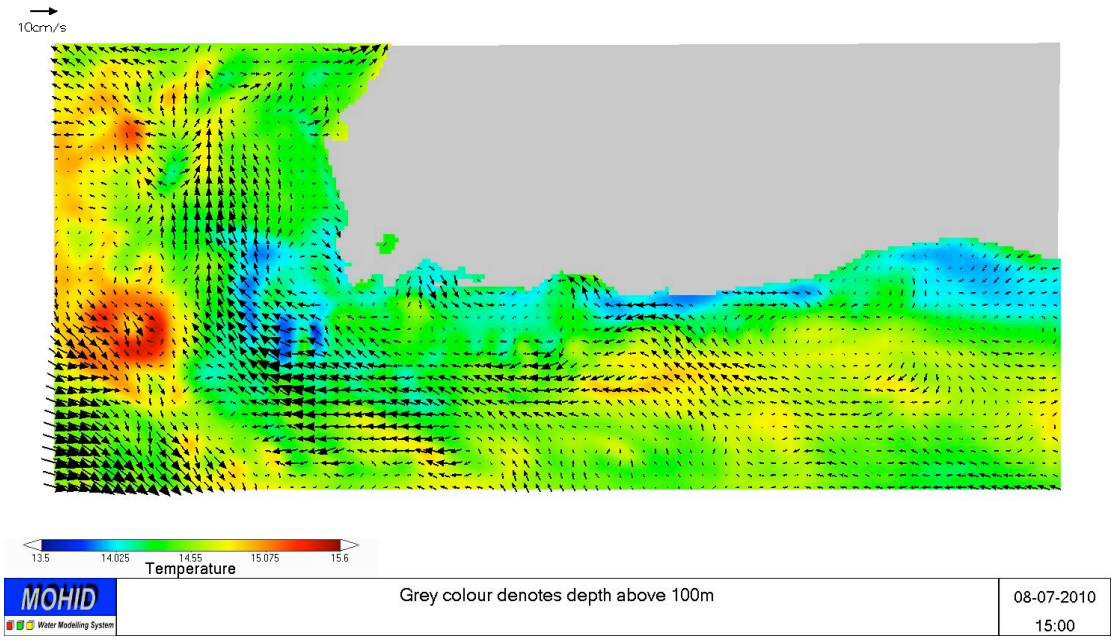

Figure 18: Depth of 100m

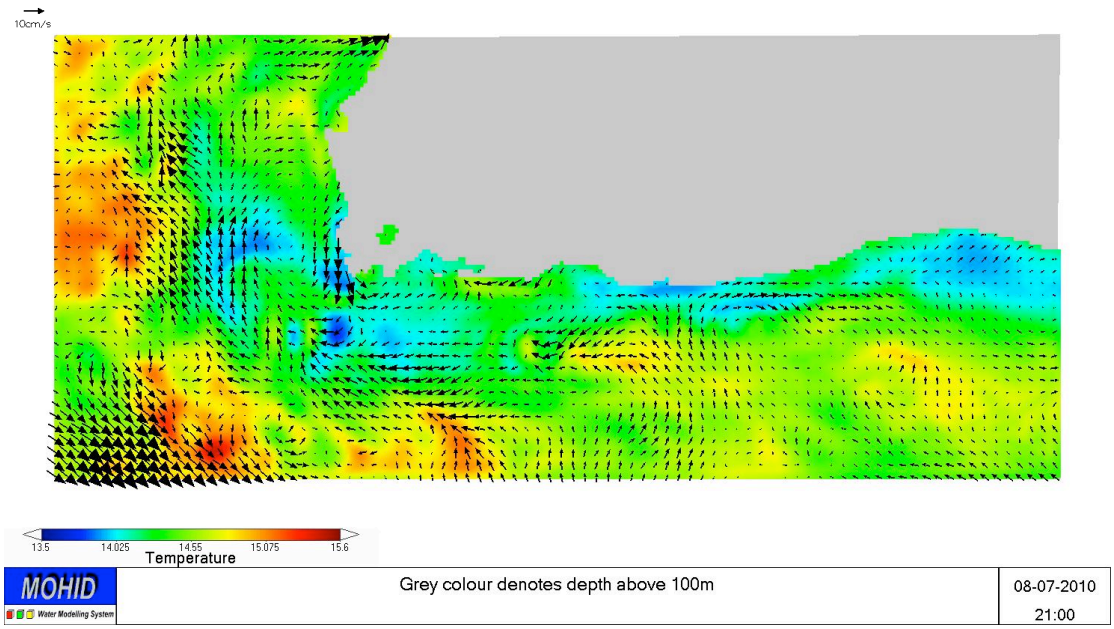

Figure 19:Depth 100m

Figure 18 and 19 both show an eddy current near to Cape St. Vincent. This eddy current was observed on several occasions throughout the simulation results always developing in close proximity to the Cape St. Vincent coast line.

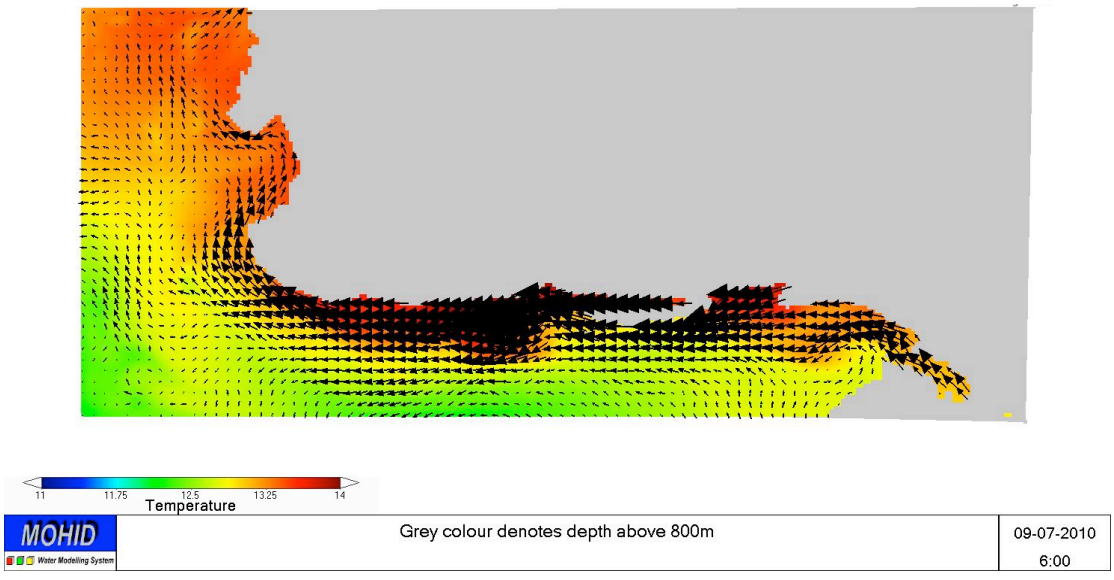

Figure 20: Depth of 800m

Figure 20 shows the hydrodynamics at a depth of approximately 800m was a typical representation of the model results for the entire simulation. There was always a strong velocity trend noted closer to the coastal boundary moving from the south east corner of the study to the north west.

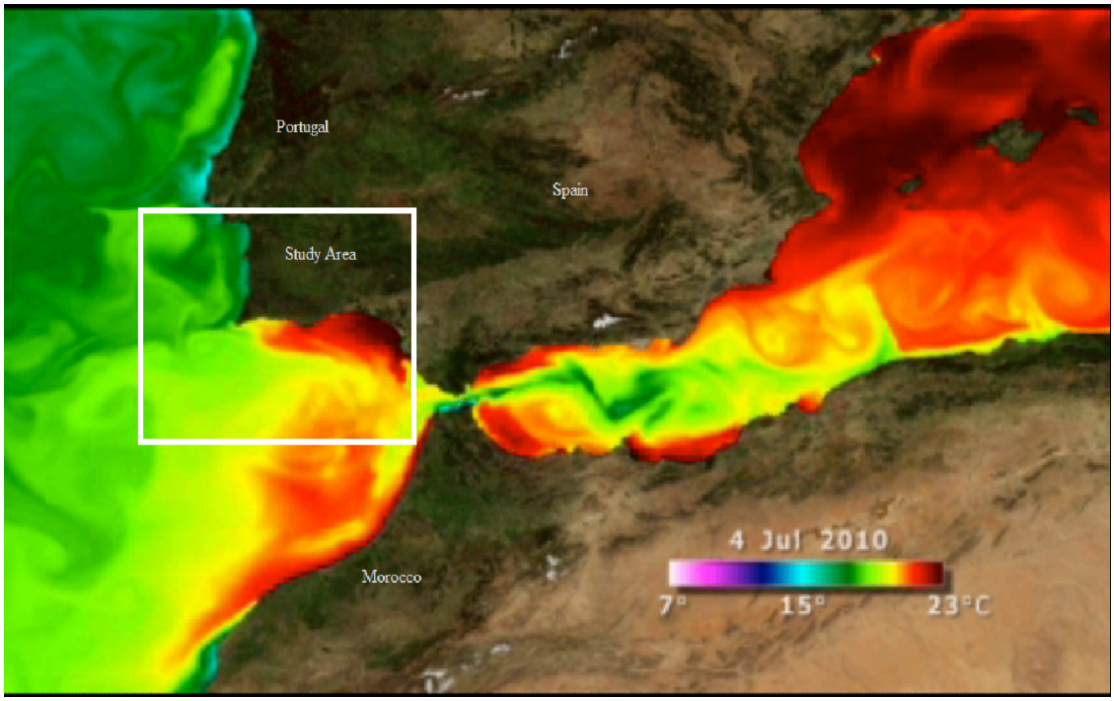

Figure 21: Satellite Image obtained from My Ocean showing sea surface temperature for Portugal, Spain and Morocco.
(http://www.myocean.eu/web/16-news-events.php?item=62) .

The satellite imagery above shows the sea surface temperature for the 4th of July. The white box denotes the general study area which was extracted and enlarged in the figure below.

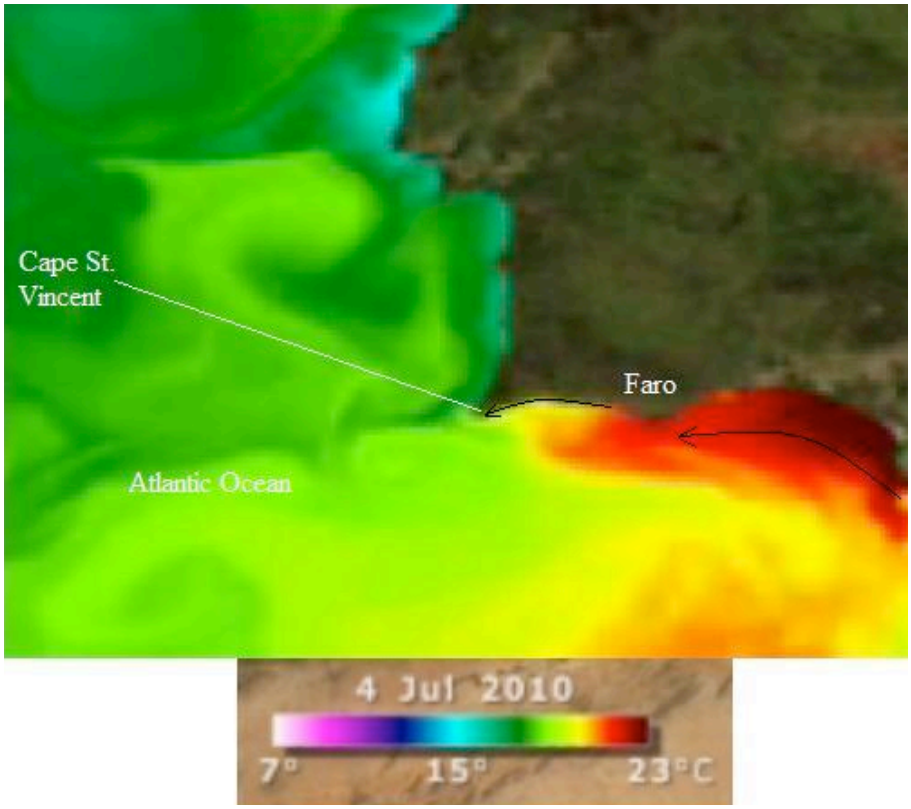

Figure 22: Showing extracted portion from previous image.

The arrows show the direction and general path the warm water body moved. This image vaguely shows the warmer water beginning to turn around Cape St. Vincent.

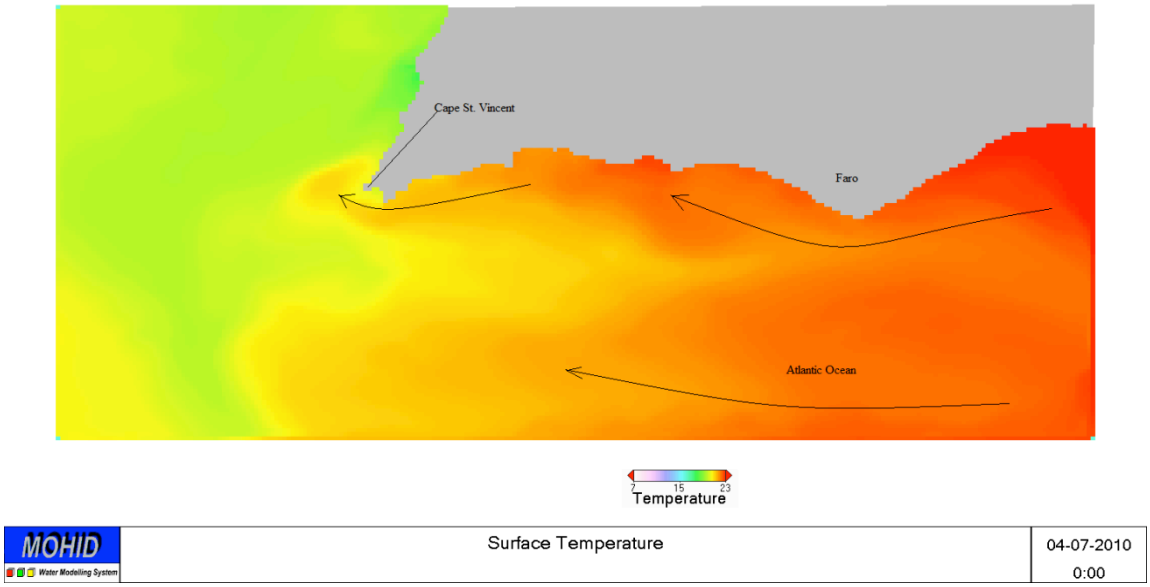

Figure 23: Image showing forecasted sea surface temperature.

The arrows show the direction and general path the warm water body moved. Figure 23 clearly shows the warmer water turning around Cape. St. Vincent. This is mainly because this image(figure 23) shows greater spatial detail than figure 22.

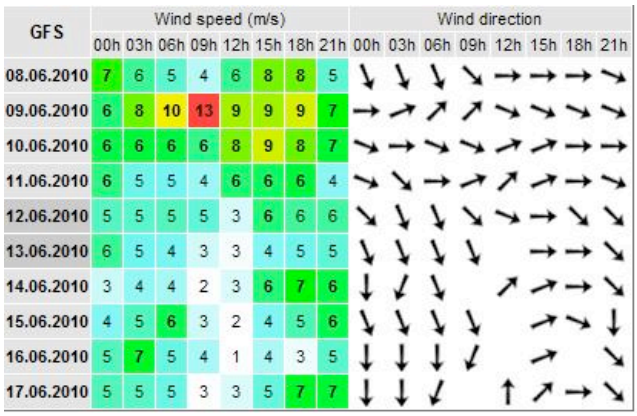

GFS	Wind speed (m/s)								Wind direction							
	00h	03h	06h	09h	12h	15h	18h	21h	00h	03h	06h	09h	12h	15h	18h	21h
08.06.2010	7	6	5	4	6	8	8	5	↘	↘	↘	↘	→	→	→	↘
09.06.2010	6	8	10	13	9	9	9	7	→	↗	↗	↗	↘	↘	↘	↘
10.06.2010	6	6	6	6	8	9	8	7	↘	→	↘	↘	↗	↗	→	→
11.06.2010	6	5	5	4	6	6	6	4	↘	↘	→	↗	↗	↗	→	↘
12.06.2010	5	5	5	5	3	6	6	6	↘	↘	↘	↘	↘	→	↘	↘
13.06.2010	6	5	4	3	3	4	5	5	↘	↘	↘	↘		→	→	↘
14.06.2010	3	4	4	2	3	6	7	6	↓	↙	↘		↗	↗	→	↘
15.06.2010	4	5	6	3	2	4	5	6	↘	↘	↘	↘		↗	↘	↓
16.06.2010	5	7	5	4	1	4	3	5	↓	↓	↓	↙		↗		↘
17.06.2010	5	5	5	3	3	5	7	7	↓	↓	↙		↑	↗	→	↘

Figure 24: Showing the daily average wind speed and Direction for the June simulation period. (Source: Wind Guru 2011)

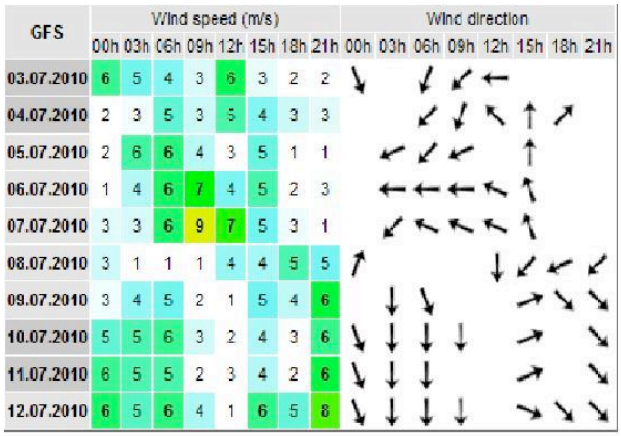

GFS	Wind speed (m/s)								Wind direction							
	00h	03h	06h	09h	12h	15h	18h	21h	00h	03h	06h	09h	12h	15h	18h	21h
03.07.2010	6	5	4	3	6	3	2	2	↘		↙	↙	←			
04.07.2010	2	3	5	3	5	4	3	3			↙	↙	↖	↑	↗	
05.07.2010	2	6	6	4	3	5	1	1		↙	↙	↙		↑		
06.07.2010	1	4	6	7	4	5	2	3		←	←	←	↖	↖		
07.07.2010	3	3	6	9	7	5	3	1		↙	↖	↖	↖	↖		
08.07.2010	3	1	1	1	4	4	5	5	↗				↓	↙	↙	↙
09.07.2010	3	4	5	2	1	5	4	6		↓	↘			↗	↘	↘
10.07.2010	5	5	6	3	2	4	3	6	↘	↓	↓	↓		↗		↘
11.07.2010	6	5	5	2	3	4	2	6	↘	↓	↓			↗		↘
12.07.2010	6	5	6	4	1	6	5	8	↘	↓	↓	↓		↘	↘	↘

Figure 25: Showing the daily average wind speed and direction for the July simulation period. (Source:Wind Guru 2011)

CHAPTER 6: Discussion and Conclusions

6.1 Tides

The difference in the forecasted and measured tidal values can be attributed to the quality of the measured tidal data. The source from which the tidal data was obtained issued this disclaimer "*The data presented under this service has not undergone any quality control and data is provided as received. The main objective is to provide a fast status assessment of station availability and performance*." (http://www.ioc-sealevelmonitoring.org/index.php)

6.2 Surface *layer*

6.2.1 June

The hydrodynamic results obtained in figures9 and 10 seem to be in agreement with those found by several authors eg . (Fiúza 1983; Barton 2001; Relvas *et al.* 2002; Sanchez *et al.* 2003). In the summer season during periods of upwelling favourable winds,(North and North-west), upwelling occurs from the west coast and travels down around Cape St. Vincent covering both eastern and western Algarve with cold upwelled water.

Relvas (2002) observed during the summer months when upwelling usually occurs, that a major filament was present to the west of Cape St. Vincent.Also, the coastal southward jet associated with the upwelling regime appears to transport cool water along the shelf break east ward around the Cape covering the Algarve with cold water. He also theorized that this frequently observed pattern could be generated by shelf edge upwelling because of the intensity of the south coast winds.

The upper surface layer is usually between 14-18.5 degrees Celsius (Fiúza 1983) and this is observed in figure 10.

Upwelling observed in summer off West Iberia, is affected by wind. As wind moves across the surface layer, water is dragged along due to frictional force and this top layer of water is pulled along in the same direction as the wind. This coupled with Ekman transport forces an upwelling of colder nutrient-rich subsurface waters along the coast. Wind-driven upwelling systems are part of the coastal upwelling occurring along the Portuguese coastline, the western coasts of the Iberian Peninsula and Africa down to 15°N (Relvas *et al.* 2002).

6.2.2 July

Figure 15 shows a reverse in the general flow of the water. In the absence of westerly winds, the coastal circulation seems to be predominantly westwards (Fiúza 1983).Intense wind blowing northerly along the western coast and westerly along the southern coast during the summer season is able to reverse the flow (Relvas 1999).This flow reached up until Cape St. Vincent and even began turning clockwise around it.

The non-upwelling pattern corresponds to the work done by (Fiúza 1983; Relvas *et al.* 2002).Both of these displayed imagery from summer periods which showed this similar event. Fiúza (1983) noticed that the cold water intrusion reduced while the warm waters close to the Algarve shore progressed in the direction of Cape St. Vincent as the intensity of the northerly winds decreased.

Relvas *et al.*(2002) completed a comprehensive analysis of wind, sea level and sea surface temperatures. They concluded that along the Portguese coast,the counter flow is driven by an alongshore pressure gradient.

They also concluded that the wind forcing can augment the flow intensity. Powerful westerly winds can reverse the alongshore current and also generate an upwelling event.

Relvas (2002) also says, if the surface temperature is used as an approximate tracer of the flow path, it may be possible to presume that this observed pattern may be dominated by a warm, coastal counter current, flowing westward along the south coast and poleward along the west coast.

6.3 100m Depth

Inner shelf circulation

Oceanographers have been paying particular attention to the inner circulation in the last decade. An example is the PISCO (Partnership for Interdisciplinary Studies of Coastal Oceans) project which focuses on the understanding of the nearshore ecosystems of the US West Coast. This region has oceanographic similarities with western Iberia (Relvas *et al.* 2007).

The interface between the populated coastline and open oceans are represented by continental shelves. This places an even great emphasis on the importance of oceanic processes. The majority of disturbances to coastal ecosystems are human induced and occurs via the inner part of the shelf. Fresh water run-off form inland also has an impact. It is increasingly being believed that the outer and inner shelf dynamics are independent of each other (Relvas *et al.* 2007).

Moving shorewards into shallower depths, it's noticed that surface and bottom boundary layer tend to overlap resulting in reduced cross-shelf transport. The physical processes that occur over the continental shelf are defined in terms of Ekman dynamics. This predicts that the cross shelf transport that occurs is directly proportional to the wind stress and alongshore currents (Relvas *et al.* 2007).

The mixed surface layer is approximately 100m in depth (Ambar *et al.* 2002). Subsurface circulation is closely liked to the circulation of the Mediterranean waters at

intermediate levels. This circulation exerts significant impact on the upper layer hydrography and dynamics off southwestern Iberia (Relvas *et al.* 2007). Coastal currents, eddy interactions with the alongshore circulation, buoyant plumes, upwelling filaments and fronts, impacts of the subsurface circulation on the upper levels and internal waves are all characteristics of this system (Relvas *et al.* 2007).

Recent studies show that Meddies can form in the surface topography.

Martins *et al.* (2002) demonstrated this by the use of drogues. The drogues were placed throughout the Atlantic encompassing Iberia. He noticed that the drogues moved in eddy circles just as seen in figures 18 and 19.

The opposing currents seen in figure 12 have no definite explanation. The mass of water which appears to be moving south-wards may be attributed to the alongshore current generated during upwelling. Ambar *et al* (2002) states that the mixed surface layer may extend up to 100m, thus the surface generated alongshore currents may penetrate to this depth.

The other mass which moves in the opposite direction travelling adjacent to the previously mentioned mass may be attributed to two things. It can be another current acting with the surface layers creating this net movement or it can be the alongshore drift associated with westerly winds. This event was noticed in both situations, both westerly and easterly dominated wind scenarios, it is more likely that this may be attributed to the subsurface influence. As stated previously Relvas *et al.*(2007) it is becoming the general perception that interaction occurs at this level.

6.4 800m Depth

During the summer season, the upper layers of water (200m) just off Iberia flow equatorward due to the equatorward winds(Baringer *et al.* 1997). The outflow splits into two cores with a shallower, along slope geostrophic component and a deeper, ageostrophic component that descends downslope (Armishaw *et al.* 2000). The flow is strongly affected by the effect of the Coriolis force which is deflecting the current to the right (looking in a downstream direction) and therefore along the slope, rather than directly west (Salles *et al.* 2007).

The undercurrent (Mediterranean Lower Water MLW) which exists within the 600-1500m depth carries Mediterranean Intermediate water, this system is called the Mediterranean Outflow. This water originates from the strait of Gibraltar and due to corolis force flows northward along the continental slope. The outflow water becomes neutrally buoyant upon mixing with the overlying fresh North Atlantic Central Water, its salinity is still well above the North Atlantic Central Water which has a similar density(Baringer *et al.* 1997).

Along its north-westerly path it intermittently separates from the coast in various locations forming subsurface eddies known as Meddies (Barton 2001).Also, the outflow registers a progressive drop in temperature, salinity and velocity.

The warmer branch of the Mediterranean Outflow (Mediterranean Upper Water: MUW), which exists between 400m-600m is the shallower core (Salles *et al.* 2007),which flows parallel to the slope in a N-NW direction.

The velocity of the MUW core is gradually reduced through the process of entrainment and mixing with the overlying North Atlantic waters. The MUW also maintained contact with the sea bed throughout its journey along the Portuguese middle continental slope of the Gulf of Cadiz(Salles *et al.* 2007).

The shear regions are typically characterized with eddies and smaller scale instablities from the poleward flow(Peliz *et al.* 2003).

The bottom topography abruptly changes direction at Cape St. Vincent. This flow separation from the bottom slope promotes the generation of Meddies. Beyond the Cape two main branches emerge from the undercurrent flowing northward and westward(Bower *et al.* 2002).

Figure 14 and figure 20 both show a strong oceanic flow bordering the coast flowing from the southeast to the northwest. The oceanic flow which was noted along the coastline was characteristically similar to that of the MLU. The model results when qualitatively compared to the literature (flow direction, flow paths and depth) were similar. In the figures a small eddy was noticed at the bottom south east corner of the system, very close to the boundary. No real assumptions could be made regarding this eddy because of its proximity to the simulation boundary, which is prone to instabilities.

6.5 Satellite Imagery

The spatial detail and clarity of the satellite image was not of the highest calibre. As a result of this, only a rough visual comparison was done between the satellite imagery and the model result for the same time period.

The arrows on both images show the general trend of the oceanic surface velocity movement of warmer water. In figure22 a warm mass of water travelling along the coastline was observed. The warm mass itself is not very clearly defined due to spatial clarity but it seems to generally conform to the shape of the coastline. Also, a ‘curl’ of warm water going around Cape St. Vincent is just barely discernable.

In figure 23 the net movement of the warm water appears to be the same. The warm water moves along the coastline and even extends as far as Cape St. Vincent. The warm

water ‘curl’ around Cape St. Vincent is easier to differentiate due to the increased level of detail.

The surface temperature results generated from MOHID appear to be a fairly close reproduction of the satellite imagery. Precise details are not clearly seen so a definitive comparison is not possible. However, the general outlook of the two images appears to be somewhat similar. They both show the same general net movement of warm water and the warm water ‘curl’ around Cape St. Vincent. Using this similarity an indicator, the results from the model at the very least are similar to that obtained from the satellite imagery.

6.6 Conclusion

The model was implemented for the study region. The qualitative analysis done between the sea surface temperature (satellite and model output) appear to show similar characteristics. A more detailed comparison was impossible due to large differences in spatial detail shown in each.

The tidal analysis revealed a noticeable difference. However, the integrity of the measured tidal data may be the underlying cause.

The overall results appear to conform to the historical data. The surface data showed both an upwelling and non-upwelling event which generally happens within the summer period.

The upwelling event which occurred during the westerly winds conforms to the historical reports. The driving forces behind the generation and direction of flow were identified from historical data as being an alongshore pressure gradient coupled with Ekman transport.

The hydrodynamic interactions observed at the 100metre depth were attributed to alongshore currents penetrating to that depth and it could also be because of interactions from the layer below.

The oceanic flow observed at 800 metres showed similar characteristics to that of the MLU. The model results when qualitatively compared to the literature (flow direction, flow paths and depth) were similar.

The MOHID model output all seem to conform to historical literature.

CHAPTER 7 : Bibliography

A lvarez-Salgado, X., et al. (2003). "The Portugal coastal counter current off NW Spain: new insights on its biogeochemical variability." Progress in Oceanography 56: 281-321.

Akin, J. E., et al. (2002). "Object-oriented Fortran 90 P-adaptive finite element method." Advances in Engineering Software 33(7-10): 461-468.

Ambar , I., et al. (2002). "Physical, chemical and sedimentological aspects of the Mediterranean outflow off Iberia,." Deep-Sea Research

Armishaw, J. E., et al. (2000). "The Barra Fan: a bottom-current reworked, glacially-fed submarine fan system." Marine and Petroleum Geology 17: 219-238.

Bajo, M., et al. (2007). "A finite element operational model for storm surge prediction in Venice." Estuarine, Coastal and Shelf Science 75(1-2): 236-249.

Baretta, J., et al. (1995). "The European regional seas ecosystem model, a complex marine ecosystem model." Netherlands Journal of Sea Research 33(3-4): 233-246.

Baringer, M. O. N., et al. (1997). "Momentum and Energy Balance of the Mediterranean Outflow." Journal of Physical Oceanography 27(8): 1678-1692.

Barton, E. (1998). "Eastern boundary of the North Atlantic: Northwest Africa and Iberia." The Sea Coastal Segment 11: 633-657.

Barton, E. (2001). Canary and Portugal Currents. Encyclopedia of Ocean Sciences. J. H. S. K. K. T. S. A. Thorpe, Academic Press. 1: 380-389.

Bischof, B., et al. (2003). "The Portugal Current System. ." "Ocean Surface Currents" http://oceancurrents.rsmas.miami.edu/atlantic/portugal.html. Retrieved 05/05, 2010.

Blayo, E., et al. (2005). "Revisiting open boundary conditions from the point of view of characteristic variables." Ocean Modelling 9(3): 231-252.

Bower, A., et al. (2002). "Structure of the Mediterranean Undercurrent and Mediterranean Water spreading around the southwestern Iberian Peninsula." JOURNAL OF GEOPHYSICAL RESEARCH 107.

Braunschweig, F., et al. (2004). "MODELAÇÃO INTEGRADA DE SISTEMAS HÍDRICOS." Portguese association of water resources.

Burchard, H., et al. (2007). "General Ocean Turbulence Model'." Retrieved 20/07, 2010, from http://www.gotm.net/index.php?go=information.

Canestrelli, P., et al. (2005). "Sea level forecasting at the Centro Previsionie Segnalazioni Maree of the Venice municipality." Cambridge University Press.

Chippada, S., et al. (1998). "A Godunov-type finite volume method for the system of Shallow water equations." Computer Methods in Applied Mechanics and Engineering 151(1-2): 105-129.

Comerma, E., et al. (2002). "An update of an oil spill model and its application in the Bay of Biscay: the weathering process " Oil and Hydrocarbon Spills III, Modelling, Analysis and Control, WIT.

Courtier, P., et al. (1991). "The ARPEGE Project at MétéoFrance." European Center for MediumRange Weather Forecast, Reading, England.

Cuehlho, H. S., et al. (2002). "A model for ocean circulation on the Iberian coast." 32: 153-179.

Daniel, P. (1996). "Operational forecasting of oil spill drift at MétéoFrance." pill Science & Technology Bulletin 3.

Daniel P, et al. (2005). Benefits and use of operational oceanography systems for drift forecasts. Proceedings of the 2005 International Oil Spill Conference, . Washington, D.C., American Petroleum Institute.

Decyk, V. K., et al. (1997). "Introduction to Object-Oriented Concepts using Fortran90 " unpublished.

Detlefsen, H., et al. (1980). "Investigations on coastal upwelling off Northwest Africa and Portugal with empirical orthogonal functions." Ocean Dynamics 33(5): 210-221.

Dias, J. A., et al. (1992). "Tidal Gauge Data in Deducing Secular Trends of Relative Sea Level and Crustal Movements in Portugal." Journal of Coastal Research 8(3): 655-659

Fiúza, A. F. Z. (1983). "Upwelling patterns off Portugal." Coastal Upwelling Part A.

Frouin, R., et al. (1990). "Observations of a poleward surface current off the coasts of Portugal and Spain during winter." Journal of Geophysical Research 95.

Hansen, S., et al. (1997). Performance and future. In "Operational Oceanography. The challenges for European Cooperation". Proceedings of the 1st International. Conference on EuroGOOS.

Harms, S., et al. (1998). "Characteristic patterns of the circulation in the Santa

Barbara Channel." Journal of Geophysical Research 103: 3041-3065.

Haynes, R., et al. (1990). "A poleward flow along the Atlantic coast of the Iberian peninsula. ." Journal of Geophysical Research 95: 11425-11441.

Haynes, R. D., et al. (1993). "Development, persistence and variability of upwelling filaments off the Atlantic coast of the Iberian Peninsula." Journal of Geophysical research 98 (C12).

Hirsch, C. (1988). Numerical computation of internal and external flows., John Wiley and Sons, Chichester.

Huthnance, J. M., et al. (2002). "Ocean margin exchange-water flux estimates." Journal of Marine Systems 32: 107-137.

Janeiro, J. (2006). Modelling hydrocarbon dispersion in two coastal ecosystems: Kongsfjord (Norway) and Patos Lagoon (Brazil). Geophysical Institute, University of Bergen. European Joint Master in Water and Coastal Management.

Jia, Y. (2000). "Formation of an azores current due to Mediterranean overflow in a modeling study of the North Atlantic." Journal of Physical Oceanography 30: 2342–2358.

Kantha, L., et al. (2000). Numerical Models Of Oceans and Oceanic Processes, ACADEMIC PRESS.

Leal, R. (2005). The regional oceanography off Cape S˜ao Vicente: from the large-scale to the upwelling filament. Faculdade de Ci^encias do Mar e do Ambiente. Faro, UNIVERSIDADE DO ALGARVE.

Leendertsee, J. J., et al. (1978). "A three-dimensional turbulent energy model for non-homogeneous estuaries and coastal sea systems." Hydrodynamics of Estuaries and Fjords(J.C.J. Nihoul Ed. Elsevier Publ. Co.,): 387-405.

Leitão, P. (2003). Integração de Escalas e Processos na Modelação do Ambiente Marinho. Dissertação para a obtenção do grau de Doutor em Engenharia do Ambiente, Instituto Superior Técnico, Lisboa.

Leitão, P., et al. (2005). "Modelling the main features of the Algarve coastal circulation during July 2004: A downscaling approach." Journal of Atmospheric & Ocean Science 10(4): 421 - 462.

Martins, C. S., et al. (2002). "Surface circulation in the eastern North Atlantic, from drifters and altimetry." J. Geophys. Res. C Oceans 107(12): 10-1.

Martins, F., et al. (2001). "3D modelling in the Sado estuary using a new generic vertical discretization approach." Oceanologica Acta 24(Supplement 1): 51-62.
Martins, P. (1999). Modelação Matemática Tridimensional de Escoamentos Costeiros e Estuarinos Usando uma Abordagem de Coordenada Vertical Genérica. Universidade Técnica de Lisboa Instituto Superior Técnico.
Martinsen, E. A., et al. (1987). "Implementation and testing of a lateral boundary scheme as an open boundary condition in a barotropic ocean model." Coastal Engineering 11(5-6): 603-627.
Miranda, R., et al. (2000). "Mohid 2000, A Costal integrated object oriened model." Hydraulic Engineering Software VIII, WIT Press.
Montero, P. (1999). Estudio de la hidrodinámica de la Ría de Vigo mediante un modelo de volúmenes finitos (Study of the hydrodynamics of the Ría de Vigo by means of a finite volume model), Universidad de Santiago de Compostela,Spain.
Moura, D., et al. (2006). "Morphological features and processes in the central Algarve rocky coast (South Portugal)." Geomorphology 81(3-4): 345-360.
Neves, et al. (2003). "Mohid Description." http://www.mohid.com/MembersArea/Downloads.asp.
Neves, R. (1985). Étude Experimentale et Modélisation dês Circulations Trasitoire et Résiduelle dans l'Estuaire du Sado. Univ. Liège.
Nittis, K., et al. (2001). "Operational Monitoring and Forecasting in the Aegean Sea: System Limitations and Forecasting Skill Evaluation." Marine Pollution Bulletin 43(7-12): 154-163.
Peliz, A., et al. (2003). "Generation and unstable evolution of a density-driven Eastern Poleward Current." Journal of Geophysical Research 108.
Peliz, A., et al. (2005). "Winter upper ocean circulation in the Western Iberian Basin - Fronts,Eddies and Poleward Flows: an overview." Deep Sea Research and Oceanographic Abstracts 52, : 621-646.
Pérez, F. F., et al. (2001). "Coupling between the Iberian basin -- scale circulation and the Portugal boundary current system: a chemical study." Deep Sea Research Part I: Oceanographic Research Papers 48(6): 1519-1533.
Pingree, R. (1993.). "Flow of surface waters to the west of the British Isles and in the Bay of Biscay." Deep Sea Research and Oceanographic Abstracts 40(12): 369-388.
Pingree, R. D., et al. (1990). "Structure, strength and seasonality of the slope currents in the Bay of Biscay region." Journal of the Marine Biology Association of
the U.K 70: 857-885.
Pollard, R. T., et al. (1985). "Structure and circulation of the Upper Atlantic Ocean northeast of the Azores." Progress in Oceanography 14: 443-462.
Poon, Y.-K., et al. (1991). "A Two-Layer Wind-Driven Coastal Circulation Model." J. Geophys. Res. 96(C2): 2535-2548.
Price, J. F., et al. (1987). "Wind-driven ocean currents and Ekman transport."
Ramp, S. R., et al. (1998). "The vertical structure of currents over the Continental Shelf off Point Sur, CA, during Spring (1990)." Deep Sea Research and Oceanographic Abstracts 45.
Relvas, P. (1999). The physical oceanography of the Cape S˜ao Vicente upwelling region observed from sea, land and space., University of Whales,Menai Bridge.
Relvas, P., et al. (2002). "Mesoscale patterns in the Cape Sa˜o Vicente (Iberian Peninsula)
upwelling region." Journal of Geophysical Research 107(C10): 3164.

Relvas, P., et al. (2005). "A separated jet and coastal counterflow during upwelling relaxation off Cape São Vicente (Iberian Peninsula)." Continental Shelf Research 25(1): 29-49.
Relvas, P., et al. (2007). "Physical oceanography of the western Iberia ecosystem: Latest views and challenges." Progress in Oceanography 74: 149-173.
Salles, T., et al. (2007). "Simulation of the interactions between gravity processes and contour currents on the Algarve Margin (South Portugal) using the stratigraphic forward model Sedsim." Sedimentary Geology In Press, Corrected Proof.
Sanchez, R. F., et al. (2003). "Spring-summer climatological circulation in the upper layer in the region of Cape St. Vincent, Southwest Portugal." ICES J. Mar. Sci. 60(6): 1232-1250.
Santos, A. J. (1995). Modelo Hidrodinâmico Tridimensional de Circulação Oceânica e Estuarina. Universidade Técnica de Lisboa, Instituto Superior Técnico.
Santos, A. M. P., et al. (2001). "Sardine and horse mackerel recruitment and upwelling off Portugal." ICES Journal of Marine Science, :
58: 589-596.
Serra, N., et al. (2005). "Observations and numerical modelling of the Mediterranean outflow splitting and eddy generation." Deep Sea Research Part II: Topical Studies in Oceanography 52(3-4): 383-408.
Silva, A. (1992). Modelação Matemática de Ondas de Superfície e de Correntes Litorais. Instituto Superior Técnico Universidade Técnica de Lisboa.
Smyth, T. J., et al. (2001). "Remote sensing of sea surface temperature and chlorophyll during Lagrangian experiments at the Iberian margin." Progress in Oceanography(51): 269-281.
Sofia, L., et al. (2005). Microplankton composition, production and upwelling dynamics in Sagres (SW Portugal) during summer of 2001.
Solignac, S., et al. (2008). "Comparison of coccolith and dinocyst assemblages in the northern North Atlantic: How well do they relate with surface hydrography?" Marine Micropaleontology 68(1-2): 115-135.
Soukissina, T., et al. (2000). "Poseidon: A marine environmental monitoring, forecasting and information system for the Greek seas." National Centre for Marine Research, Institute of Oceanography.
Sousa, F. M., et al. (1992). "Satellite-derived phytoplankton pigment structures in the Portuguese upwelling area." Journal of Geophysical Research 97: 11343-11356.
Strub, P. T., et al. (1991). "The Nature of the Cold Filaments in the California Current System." J. Geophys. Res 96(C8)(14): 743-14.
Torres, R., et al. (2003). "Spatial patterns of wind and sea surface temperature in the Galician upwelling region." Journal of Geophysical Research 108(C4).
Tucker , A., et al. (2004). Computer science handbook, The Associatioon for computeing machinery.
UNESCO (1981). "Tenth Report on the joint panel on oceanographic tables and standards." Technical papers in marine science, 36(24).
Welch, G., et al. (2006). An introduction to the Kalman Filter., Department of Computer Science
University of North Carolina at Chapel Hill
Chapel Hill, NC 27599-3175

Wooster, W., et al. (1976). "The seasonal upwelling cycle along the eastern boundary of the North Atlantic." Journal of Marine Research 34(2): 131-141.

Appendice 1

Images showing the gradual Progression of the Upwelling event.

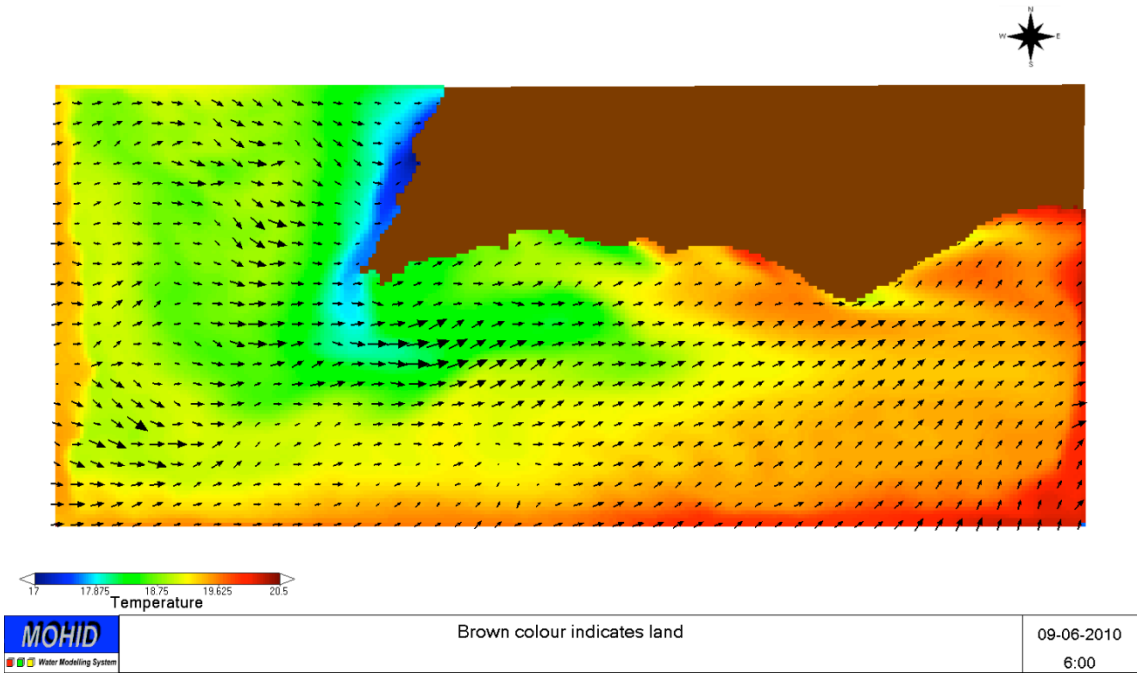

Figure 26

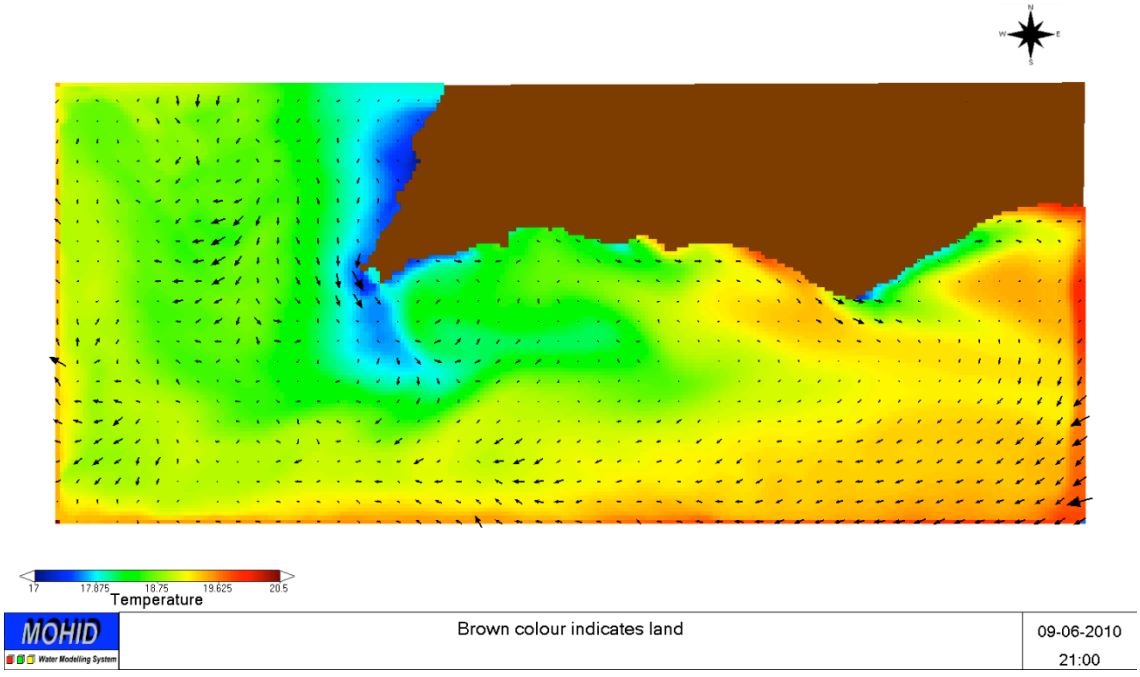

Figure 27

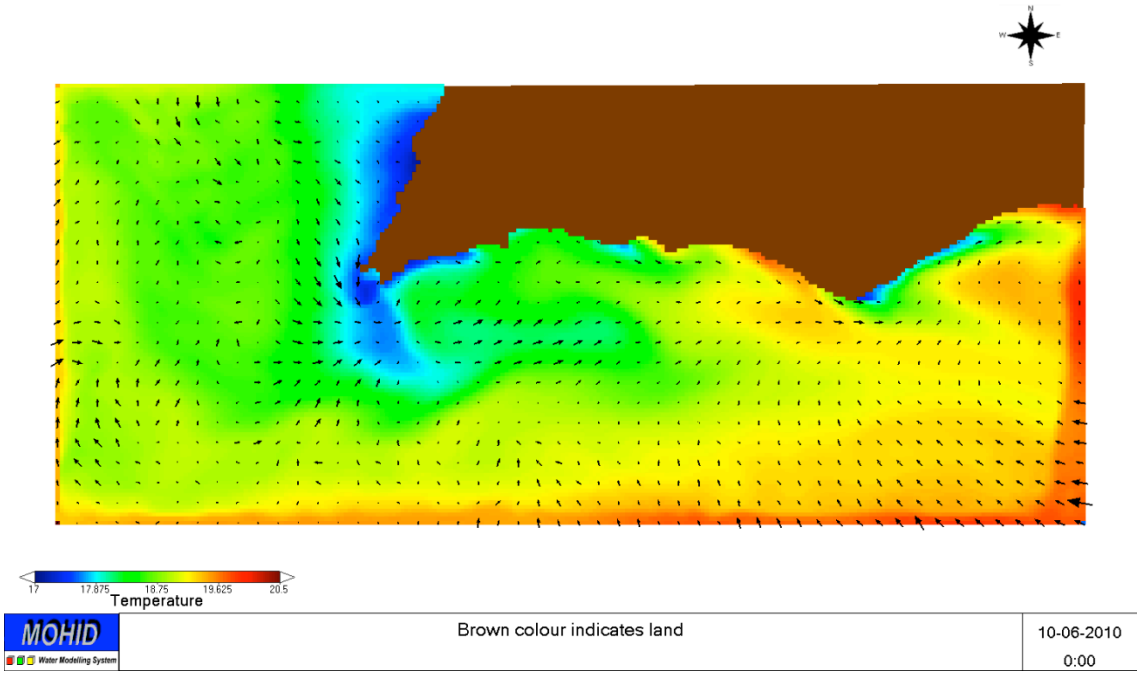

Figure 28

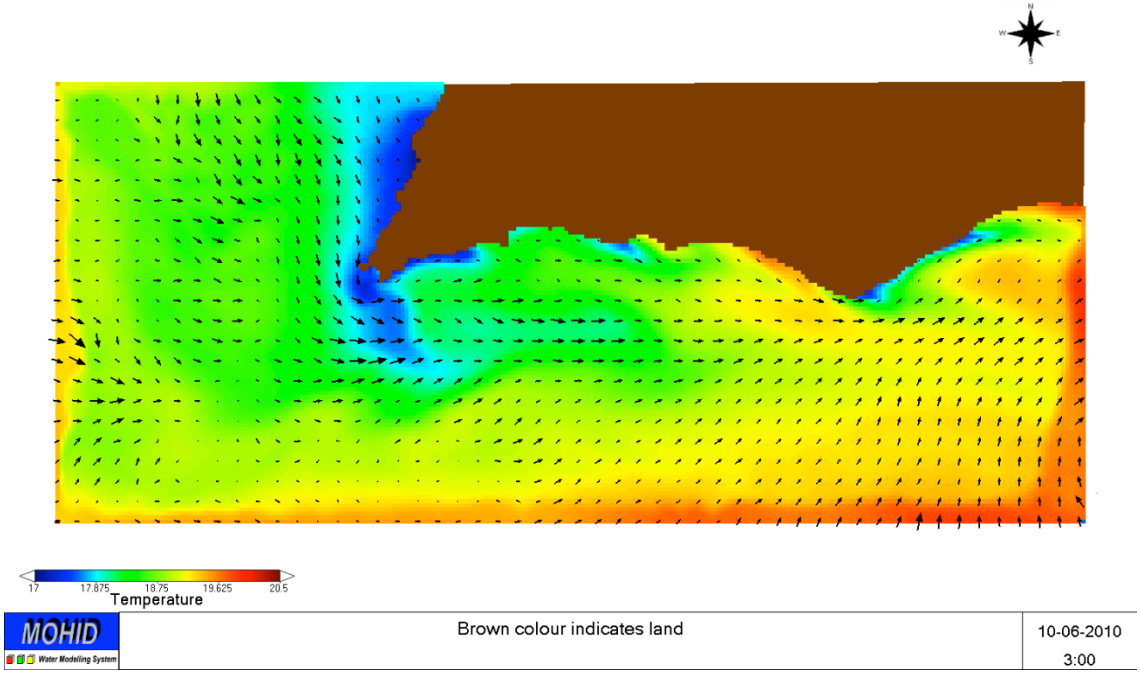

Figure 29

Appendix 2

Showing the spatial movement of the velocity vortex

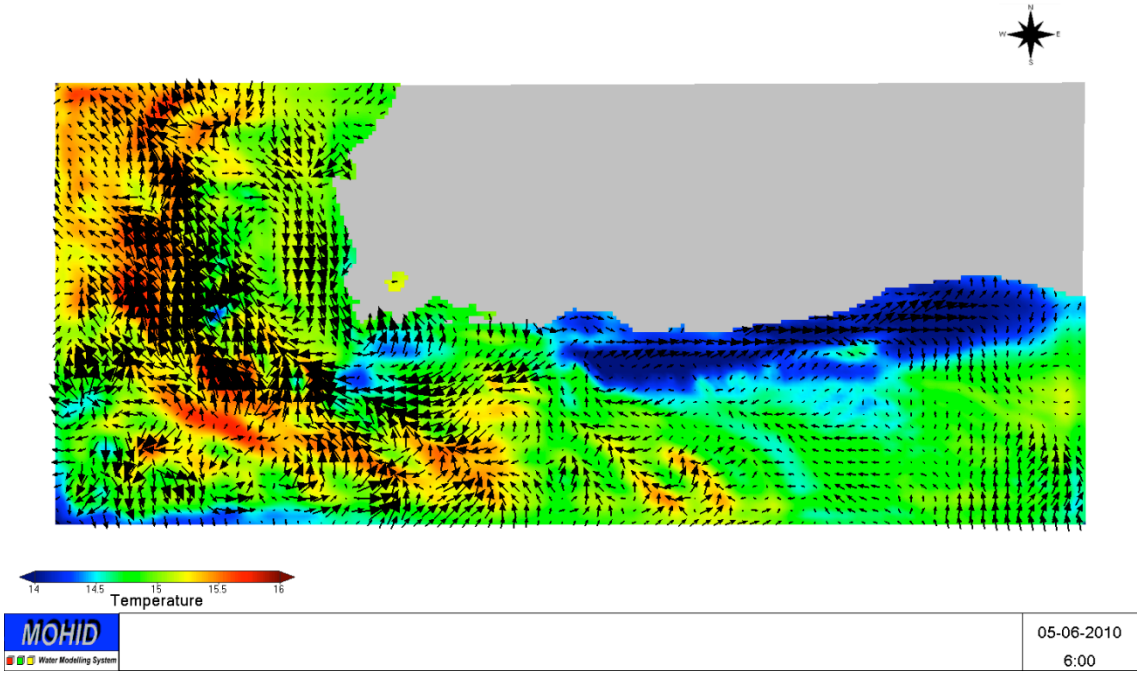

Figure 30

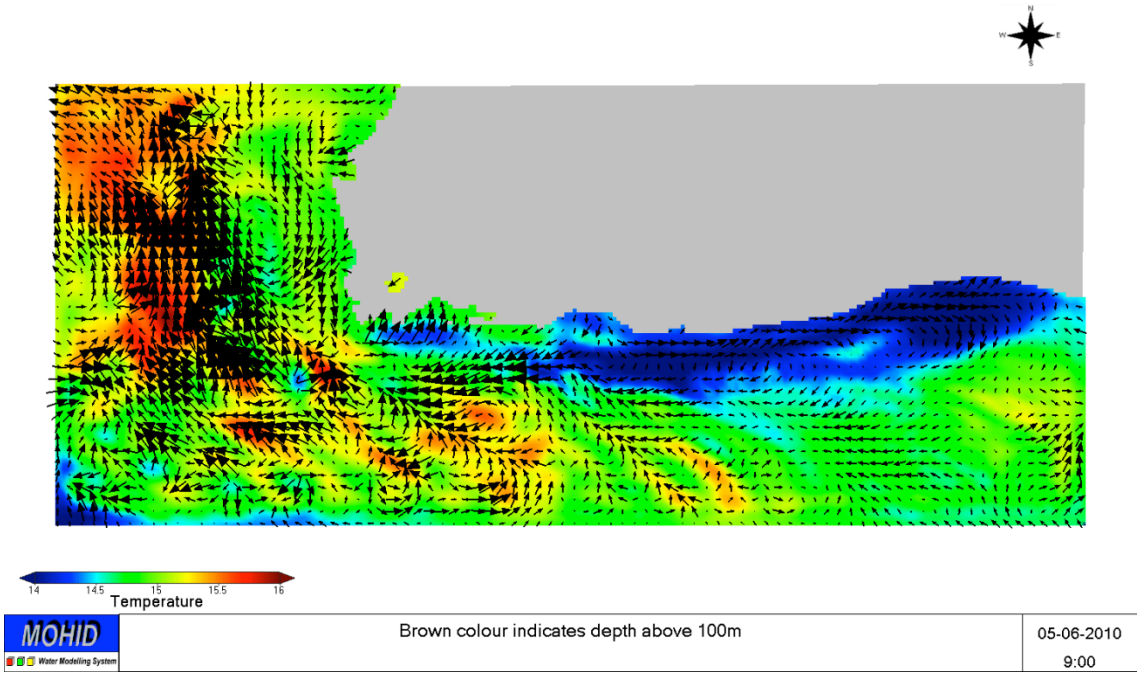

Figure 31

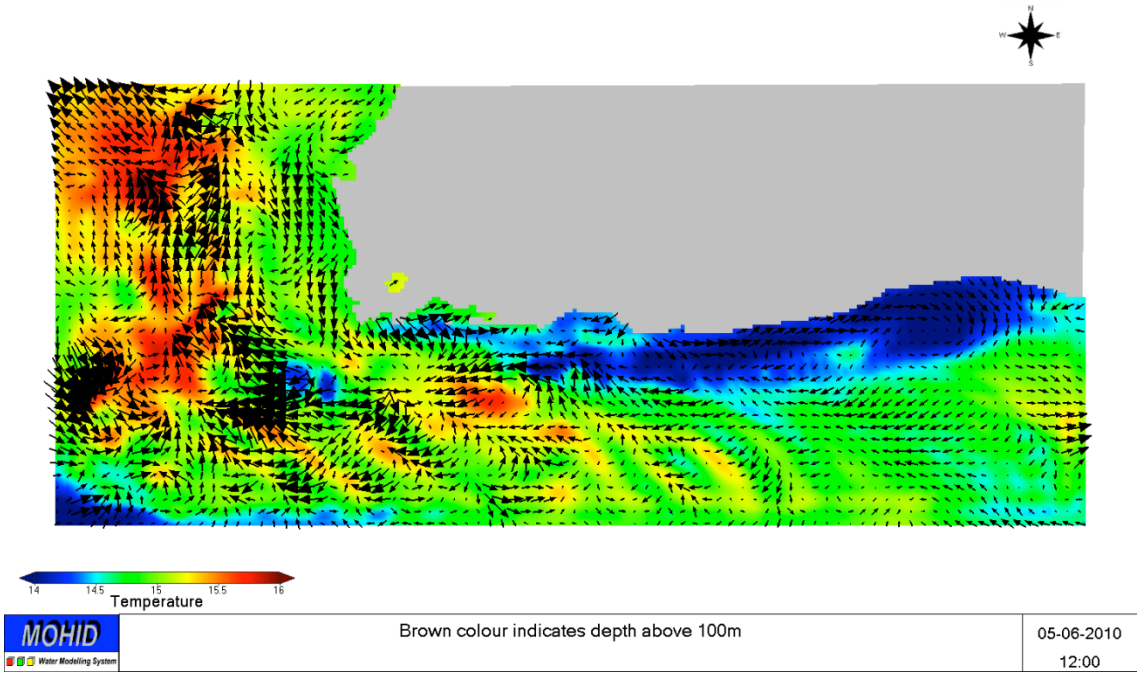

Figure 32

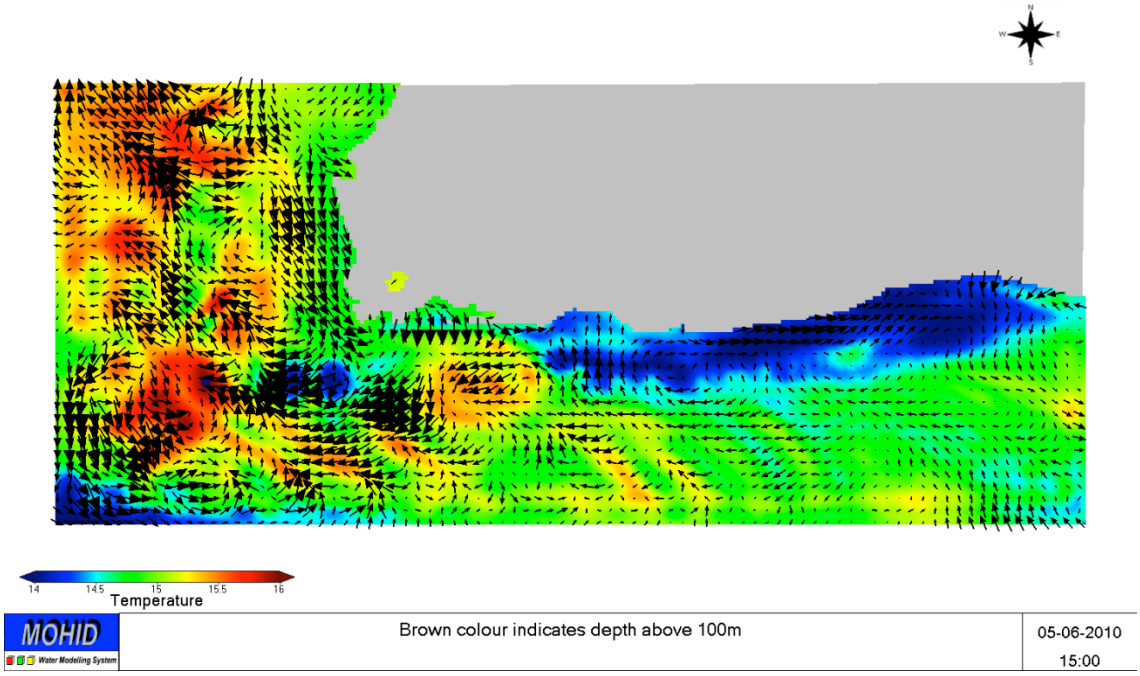

Figure 33

Appendix 3

Showing the velocity vortex observed in both June and July respectively.

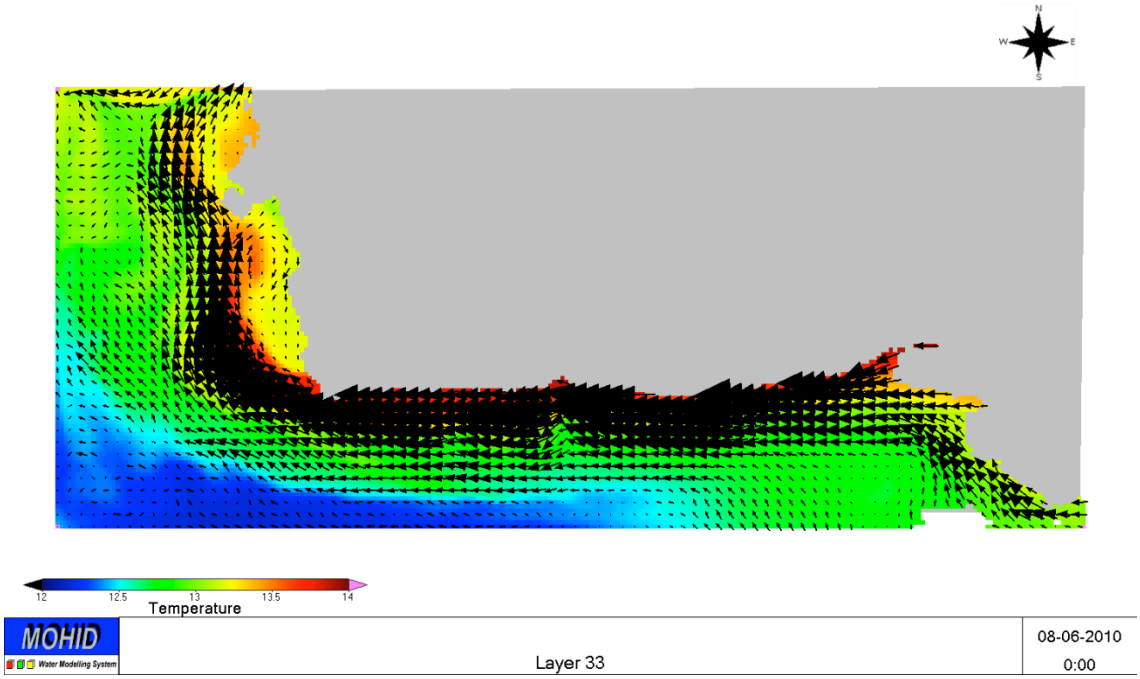

Figure 34

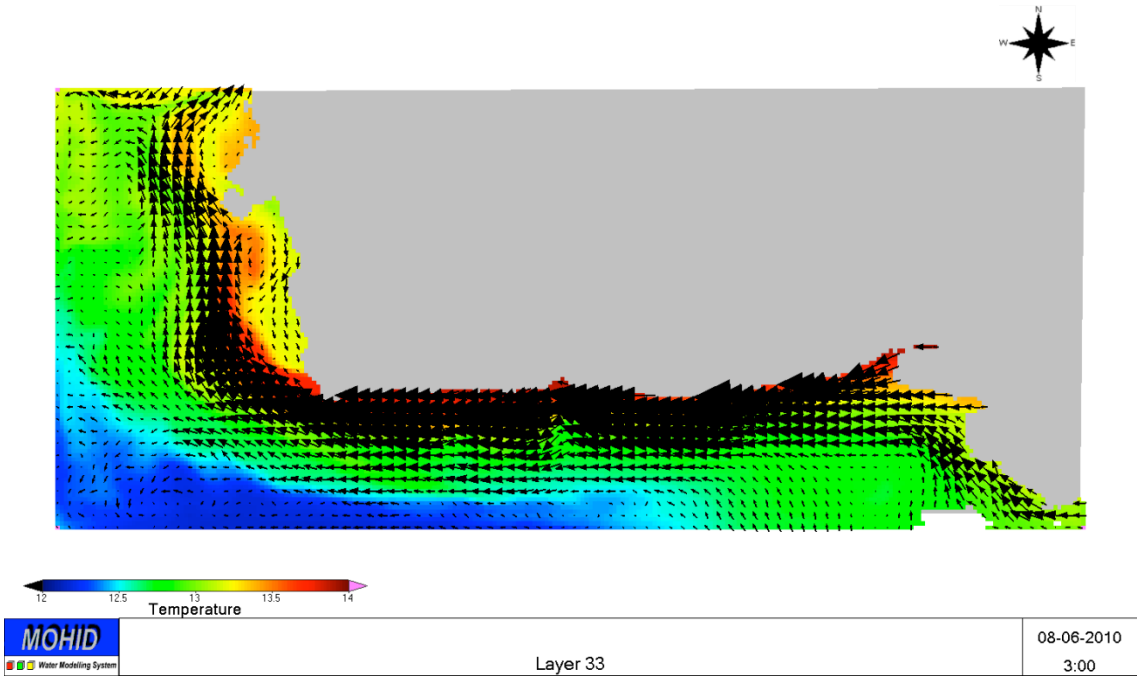

Figure 35

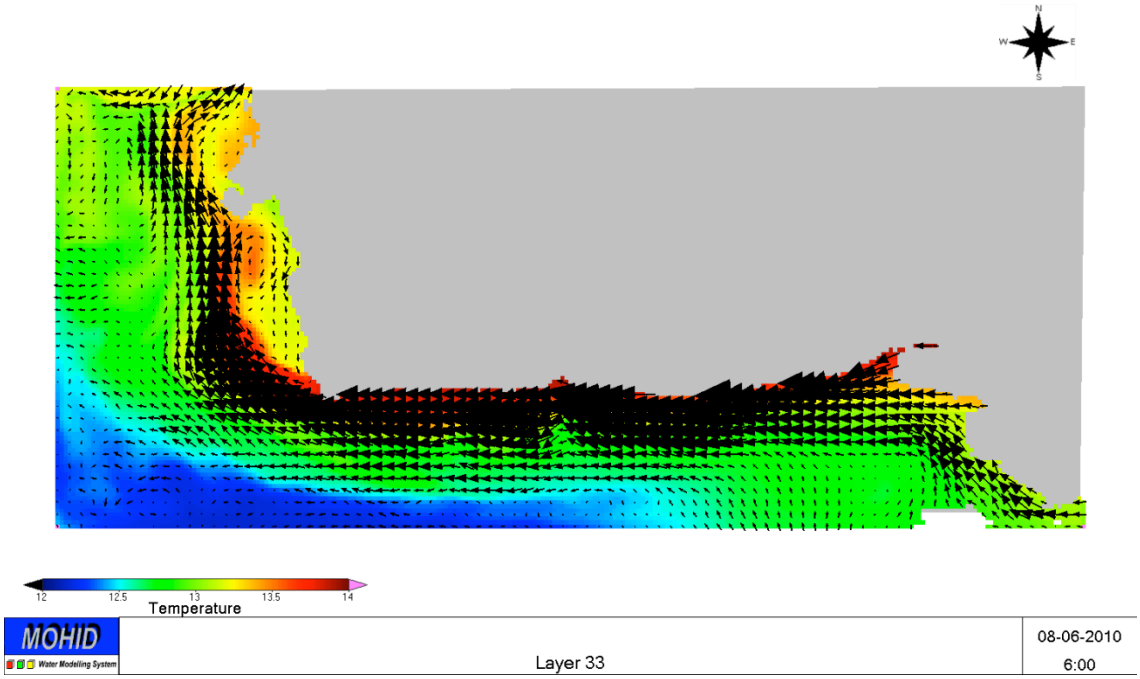

Figure 36

July

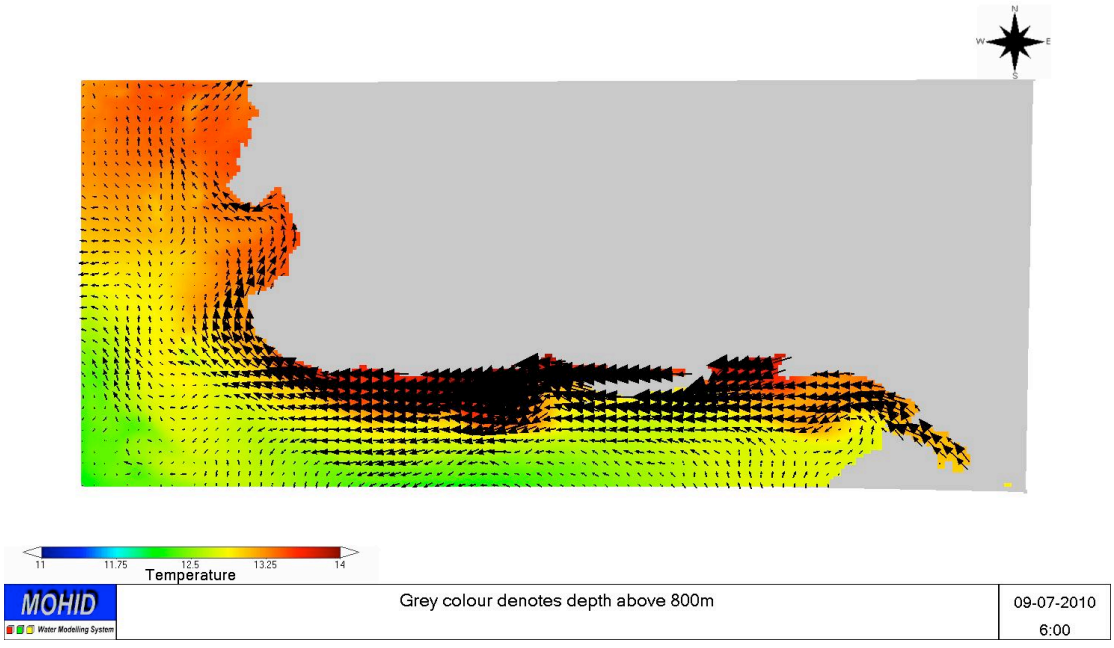

Figure 37

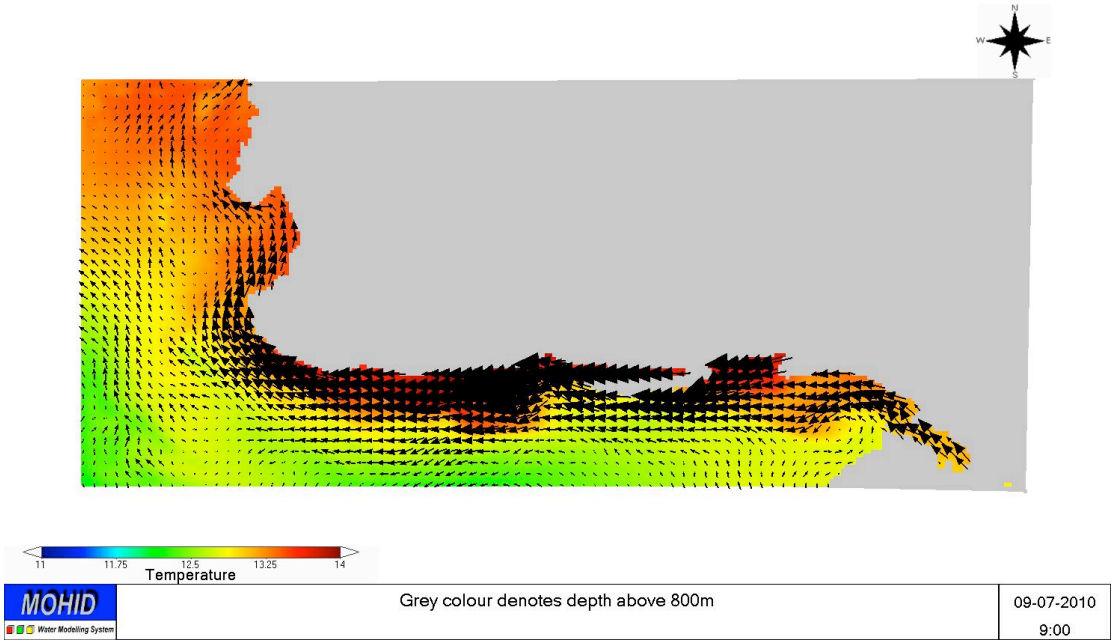

Figure 38

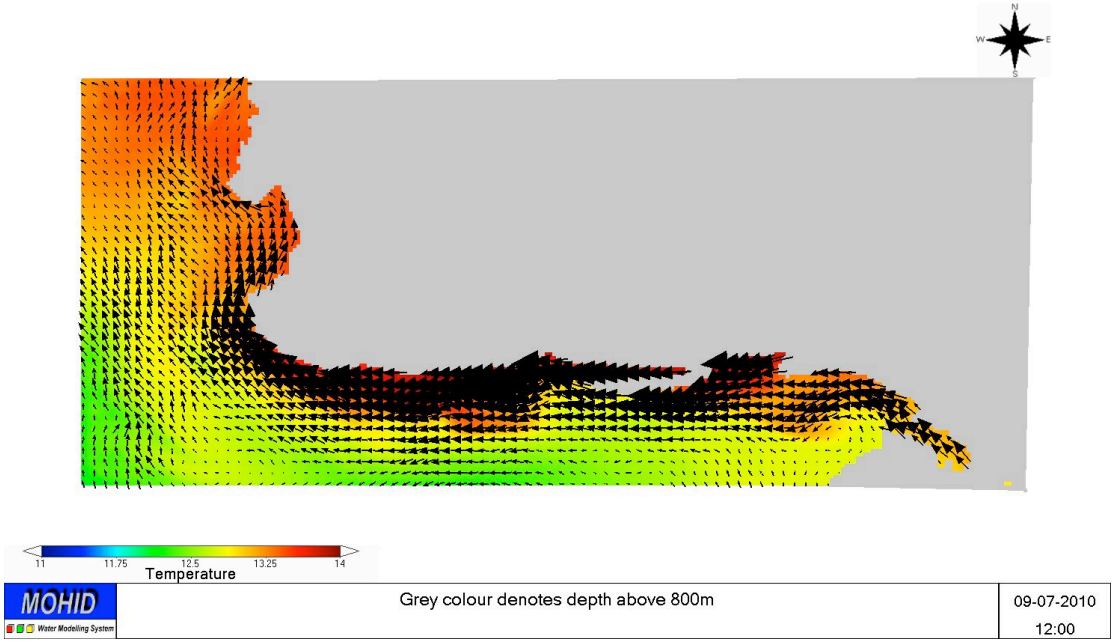

Figure 39